Università di Pisa

Facoltà di Scienze Matematiche Fisiche e Naturali

Corso di Laurea Magistrale in Fisica

Anno Accademico 2010/2011

Tesi di Laurea Magistrale

High Power Laser-Grating Interaction

Candidato: Mattia LUPETTI

Relatore: Caterina RICONDA
Relatore: Andrea MACCHI

Ringraziamenti

Ai miei relatori: a Caterina, per il continuo incoraggiamento nonostante la situazione drammatica dei codici, e ad Andrea, per la paziente gentilezza che mi ha sempre rivolto.

A Tommaso, per il backup informatico e le grigliate salva-domenica.

Agli inventori dell'Erasmus, per avermi fatto vivere un'esperienza sopra le righe

Agli amici dell'università, perché è sempre un piacere tornare a Pisa

Al mio paese, per le varie lezioni di vita

Alla mia famiglia, per la vita meravigliosa che mi ha regalato

Alla mia ragazza, per aver condiviso con me tutto quello che ho appena scritto

Contents

Chapter 1

Introduction

1.1 Overview

It is well known that when a flat metallic surface is shone with light whose frequency is in the optical range, it behaves like a perfect mirror, i.e. reflecting back with the same angle of incidence the impinging light ray. The requirement for a metallic surface to be considered a perfect mirror is that on the microscopic scale, the surface imperfections are much smaller than the incident light wavelength. If that's not the case, the electromagnetic field lines at the metal surface are bent according to the local surface normal, and thus a clear image doesn't form, since "specular" reflection is no more occurring.
But if from the surface "roughness" it is possible to extract a leading component of *periodicity* d, of the same order of magnitude of the wavelength λ, then a whole new bunch of more complicated physics phenomena appears and are commonly studied in optics.
Indeed, a surface which presents a periodic optical structure is also named a photonic structure, and it allows one to manipulate light in much more evolved ways than with a flat mirror. The most simple one dimensional photonic structure that can be made of metallic material is a *diffraction grating*, which is known for its "light splitting" properties: since the angles at which light is reflected depends on λ/d, each different wavelength forming the incident wave-packet will be reflected at a different angle. However, for particular conditions of the incident light and λ/d ratio, a diffraction grating can behaves like an optical cavity (see chapter 3), i.e. all the incident light can be confined in the proximity of the grating surface and converted into a *surface wave*, a kind of wave that propagates parallel to the metallic surface and is evanescent away from it.
The possibility of exciting those kind of surface modes, and their remarkable properties, have been successfully applied to a broad variety of fields ranging from the engineering of biosensors in biophysics to the construction of low dimensional wave guides in optics. All these applications are investigated in the research field commonly known as *plasmonics* (see for example [Maier 2007]), from the physical origin of the excitation of those modes: indeed, for a given frequency, the electrons at the grating surface can oscillate coherently in a way similar to the collective motion of bulk electrons in a "plasmon" wave. Hence, in solid state physics these surface waves are usually called *surface plasmon resonances* or *surface plasmon-polariton*. In the present work, because of its multidisciplinary approach, we will freely use the terms "surface wave", "surface mode", "surface plasmon" or "surface plasmon resonance" with the same meaning, but in the context where they are more appropriate.
Surface plasmon resonances (SPR), because of the enhancement of the e.m. field they provide, have been tentatively employed also in high energy physics, the interest here being the possibility to better accelerate charged particles. We will present in the next

two paragraphs how this idea has evolved till nowadays.

1.2 From the grating accelerator concept...

The idea of accelerating particles in the fields produced in proximity of a metallic surface came first to light in the 60s to high energy physicists in the attempt to accelerate electrons up to GeV energy in accelerators *much smaller* than the existing ones. To obtain smaller dimensions, the first step would be to substitute the radio frequency power sources with lasers sources. This would permit to miniaturize the typical accelerating unit from a length of the order of 10 cm, down to the μm length scale! Unfortunately, it is not possible to accelerate particles (electrons) directly with a laser field (Lawson-Woodward theorem), so the idea was to use evanescent optical modes close to a photonic structure, in order to control non-relativistic electrons. Since the acceleration had to occur on a straight line (they wanted a linear accelerator), the most simple 1D photonic structure to choose was a *diffraction grating*.
The key idea in the use of a diffraction grating is that in order to accelerate electron parallel to the surface one has to convert the transversal electromagnetic waves travelling at c velocity into "slower" longitudinal modes, having the electric field component in the desired direction.
Moreover it had been demonstrated in 1953 that when particles travel over the surface of a grating, light is emitted [Smith 1953]. It seemed reasonable, therefore, that in 1968 Takeda and Matsui should propose what they believed to be the inverse of this effect as an accelerator concept [Takeda 1968].

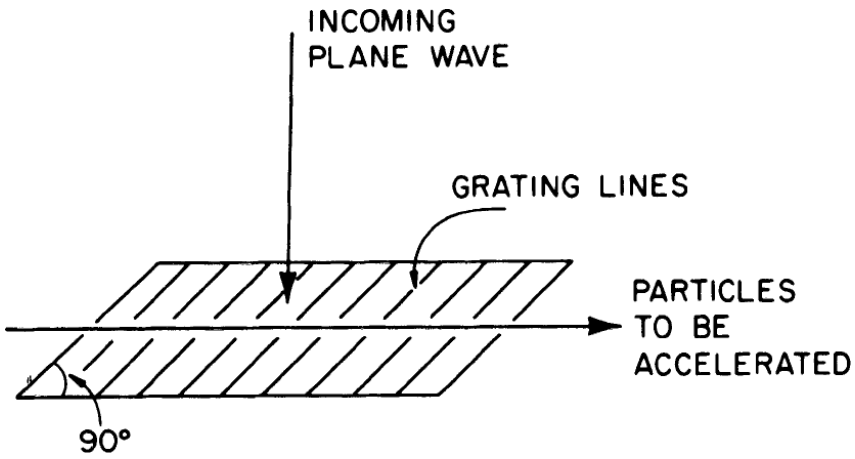

Figure 1.1: Scheme of a grating accelerator. The electric field of the incident laser beam is orthogonal to the grating lines, in oder to accelerate the charged particles in the desired direction

Unfortunately, and we'll show it in chapter 2.4, it can be proved that the proposed geometry would not work for relativistic particles [Lawson 1979]. It was not until 1980 that Palmer demonstrated that it was only for the particular geometry of Takeda and Matsui that Lawson's criticism applied and that for skew or otherwise more three dimensional geometries acceleration could indeed be obtained [Palmer 1980]. It was shown further

that the grating, if given the right periodicity, could act as a true "cavity". That is, it had accelerating modes that *were restricted to the surface* and did not radiate energy away from that surface.

One of the biggest problem on this "laser accelerator" concept was that the field necessary to accelerate electrons to the required energies would inevitably destroy the metal grating. Nowadays, work on laser accelerators is still fervent, but is based on dielectric gratings instead of metal ones. This design, which was introduced by Plettner, consists of a pair of opposing transparent binary gratings [Plettner 2005].

1.3 ...to "grating assisted" heating

Another research field that involves the concept of particle acceleration in surface fields is high power laser-matter interaction.

Today's amplification laser technologies is such that a PetaWatt laser pulse can be delivered in a time interval shorter than a picosecond. In these conditions ordinary matter is rapidly ionized and forms a high density plasma in front of the laser target. Thus, there will be free electrons that can be accelerated by surface waves.

Moreover, when the target used in experiments is a solid one, the electron density is greater then the critical density (or cut off density)

$$n_{cr}(\omega) = \frac{m_e \omega^2}{4\pi e^2} \simeq 1.1 \times 10^{21} \times \left(\frac{\lambda}{1\ \mu\mathrm{m}}\right)^2\ \mathrm{cm}^{-3}$$

i.e. the density over which no propagation of light in the medium can occur. Thus, no propagation of light can occur *inside* the material and the preformed plasma is said to be *overdense*.

This is the typical situation, for example, in fast ignition concept [Atzeni 2004] or electron and ion acceleration from thin targets [Borghesi 2006]. Since light cannot propagate inside the material, the key feature in all these applications is to find an efficient way to convert the laser power into energy transferred to the material. Moreover, such high power lasers can heat the electrons to a temperature of the order of keVs, thus making further Ohmic heating, or collisional heating, more and more difficult, because the resistivity will become smaller and smaller for rising temperature (Spitzer). To overcome this limitation, a (great) number of collisionless energy transfer mechanisms have been studied (see for example [Kruer 1985], [Brunel 1987], [Gibbon 1992]) and they are based on the fact that strong energy absorption can be accounted for by the electrons that are dragged in the vacuum and sent back into the plasma with supra thermal velocities.

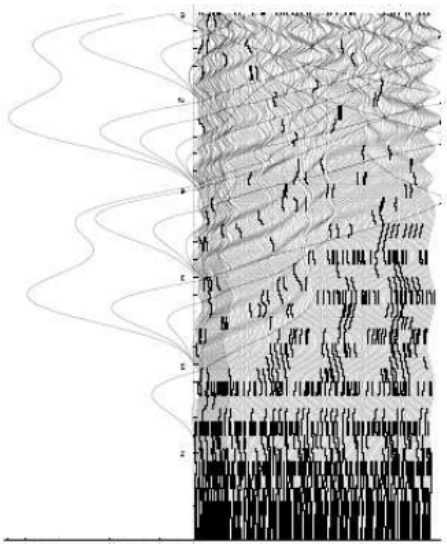

Figure 1.2: Numerical simulation of the Brunel effect. In the figure, electrons crossing the surface are observed to spend one or two oscillation periods on the vacuum side, and then re-enter into the plasma slab at high velocity. In this way, electron jets are produced once per cycle

It is worth reporting that Brunel itself, in his highly cited paper "Not-so-resonant, resonant absorption" where he invented what was after called "Brunel effect" (see fig. 1.2), was motivated by the importance those injected fast electrons could have in a grating accelerator scenario:

> This mechanism is effective when the overdense plasma density is well over the critical density and when a strong density gradient or discontinuity is present; the presence of an underdense plasma is not necessary. Those conditions are met in the laser grating accelerator concept, where an intense laser field incident on a grating is used to accelerate electrons.

He concluded that the presence of electrons accelerated into the material, that caused a part of the laser energy to be absorbed, could lead to a damping of the surface waves that were necessary to accelerate particles *along* the surface.
Thus, it is of some effect remarking that what was born as an attempt to "smooth down" the energy absorption due to fast electrons injection into the material, has now become a new route to increase the energy absorption itself. The idea of improving the laser coupling with the target by using a structured surface is supported by successful experiments in the low energy counterpart, where is well established that peaks of photoelectrons emission are observed in correspondence with the resonant excitation of surface modes (see for example [Irvine 2006], [Liu 2007], [Stockman 2007]).
The same effort has been made also in high power laser matter interaction, with experimental work carried out by [Kupersztych 2001] and later [Bastiani-Ceccotti 2003]. The main experimental limitation here is that the laser pre-pulse, the long duration low power part preceding the power peak, tends to deform and corrupt the modulating structure before the interaction with the peak laser pulse occur. However, later self-consistent particle-in-cell simulations (see for example [Raynaud 2007]), have confirmed that for p-polarised

incident light the absorption coefficient rises from the nearly 20% of a flat surface to the 70% achieved when using a modulated surface. The interest in carrying out this work lies in the fact that nowadays high contrast laser pulses with much weaker pre-pulses are available (recently the experimental project "Ultrahigh Contrast Laser Interaction with Structured Targets" on SLIC UHI laser facility has been accepted by the LASERLAB EUROPE Selection Panel, see [Macchi]).
But since no clear experimental validation of the role played by surface modes excitation in the absorption enhancement through hot electrons acceleration is available yet, the main criticisms those simulation works received have been that the same enhancing effect could be caused by "curvature" of the modulated surface, which tends to periodically focalize the fields in "hot spots" in front of the grating, where the field intensity can easily be greater than two times the incident field amplitude. Thus, a higher potential is available for those "lucky" electrons which are in phase with the potential peak.
The shortcoming with particle-in-cell (PIC) simulations (for example in [Bigongiari 2011]) is that the surface modes contribution it's not clearly distinguishable, because too many transfer mechanisms are involved. Therefore, it is difficult to answer to the above criticism according to PIC simulations only.

1.4 Outline of this work

Therefore, the aim of this work is to try to clarify which is the physics involved in electrons acceleration into the target when a structured surface is present. We will use the following approach:

- ▷ The optical response of the overdense plasma is described by the dielectric function of a classical Drude metal.
- ▷ The fields in proximity of the grating surface are studied with an electromagnetic code that employs a finite-difference time-domain (FDTD) algorithm
- ▷ The electrons acceleration is studied with a test particle approach: the underlying hypothesis is that the number density of the accelerated particles n_{fast} is much smaller than the electron density n_e. In this approximation it is possible to neglect the e.m. fields induced by the fast electrons motion

In the second chapter we will analyse in detail the fundamentals of the simplest structured surface, i.e. a sinusoidal diffraction grating, and we'll report different methods to obtain analytical solutions of the diffracted fields *in proximity* of the material surface. In the third chapter a detailed study on surface "resonant" modes excitation is presented, together with an analytical model to account for the effects due to the grating geometry. Thank to this, we have derived a formula which is able to predict the resonant frequency shift caused by the increasing of the grating amplitude:

$$\overline{\omega} = \omega_{res}\left[1 - \left(\frac{hq}{4}\right)^2\right] \qquad \text{for grating profile } f(x) = \frac{h}{2}\cos(qx), \quad q = \frac{2\pi}{d} \tag{1.1}$$

In the fourth chapter the dynamics of the accelerated particles is studied with the help of numerical simulations. We are able to show that the electrons dynamics is greatly sensitive to SPR excitation. In particular, the average kinetic energy acquired by the electrons in the resonant fields is much greater than in the not resonant case, and the energy distribution of the accelerated electrons shows an extended "plateau" region that is absent when the resonance is not excited.
This confirms our hypothesis that the major effect in electrons acceleration grating driven enhancement is due to the possibility to excite collective surface electrons modes, and cannot be explained as a consequence of "hot spot" creation in the field pattern, because of the field lines bending caused by the modulation of the surface. Consequently the energy absorption enhancement observed in PIC simulations has to be considered an effect of the collective surface electron mode excitation.

Chapter 2

Diffraction gratings

In this chapter we illustrate the basic theory of the diffraction problem and different approach to treat the boundary conditions

2.1 Scalar theory of diffraction gratings

The diffraction problem of a plane wave impinging on a perfectly conducting grating can be described by imposing that the field produced in vacuum by the incident waves

$$\mathbf{E}_{in} = \hat{\mathbf{a}}\, E_0\, e^{i\mathbf{k}\cdot\mathbf{r} - i\omega t} \tag{2.1}$$

$$\mathbf{B}_{in} = \hat{\mathbf{b}}\, E_0\, e^{i\mathbf{k}\cdot\mathbf{r} - i\omega t} \tag{2.2}$$

where

$$\begin{cases} \mathbf{r} = (x, y, z) \\ \mathbf{k} = (k\sin\theta\sin\phi, -k\cos\theta\sin\phi, -k\cos\phi) \\ \hat{\mathbf{b}} = \dfrac{c\mathbf{k}\times\hat{\mathbf{a}}}{\omega} \quad \Longrightarrow \quad \hat{\mathbf{a}}\cdot\mathbf{k} = \hat{\mathbf{b}}\cdot\mathbf{k} = 0 \end{cases} \tag{2.3}$$

satisfies Maxwell equations:

$$\nabla\times\mathbf{E}^d = \frac{i\omega}{c}\mathbf{B}^d \qquad \nabla\times\mathbf{B}^d = -\frac{i\omega}{c}\mathbf{E}^d \tag{2.4}$$

$$\nabla\cdot\mathbf{E}^d = 0 \qquad \nabla\cdot\mathbf{B}^d = 0 \tag{2.5}$$

where I defined

$$\mathbf{E}^d = \mathbf{E} - \mathbf{E}_{in} \tag{2.6}$$

$$\mathbf{B}^d = \mathbf{B} - \mathbf{B}_{in} \tag{2.7}$$

A general solution of this problem requires a vector formalism we are not interested in. To make things simple, let the vector $\mathbf{k}$ lie in the (x, y) plane, and let the grid profile Γ be invariant along the $\hat{z}$-direction, so that it can be described by the function $y = f(x)$ of period d. The geometry of the problem, now reduced to 2D, is shown in figure 2.1:
Within this framework, since now $\partial_z = 0$, Maxwell equations plus boundary conditions (BCs) read:

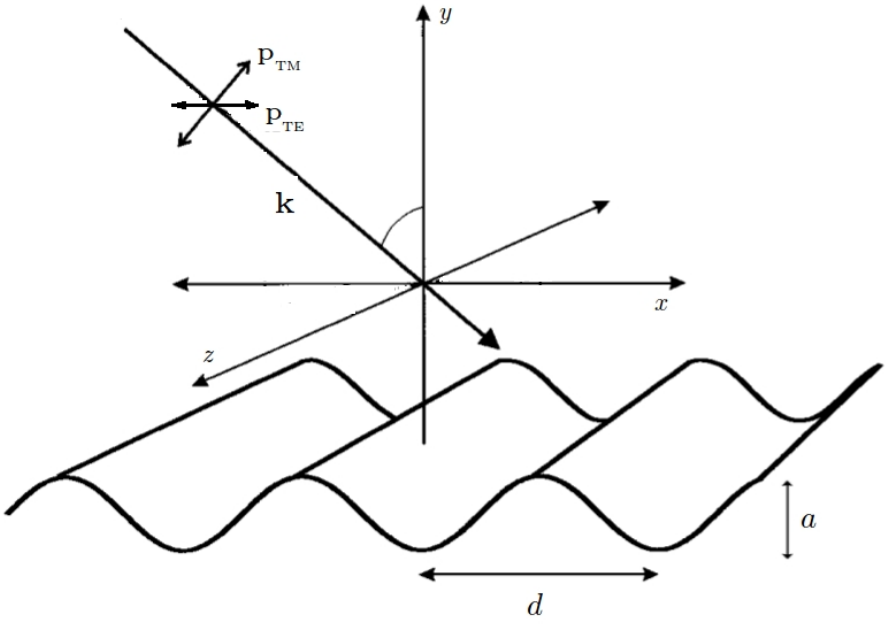

Figure 2.1: Simplified diffraction geometry

$$\begin{aligned} \partial_y E_z^d &= ikB_x^d \\ \partial_x E_z^d &= -ikB_y^d \\ \partial_x E_y^d - \partial_y E_x^d &= ikB_z^d \\ \partial_y B_z^d &= -ikE_x^d \\ \partial_x B_z^d &= ikE_y^d \\ \partial_x B_y^d - \partial_y B_x^d &= -ikE_z^d \end{aligned} \qquad \text{with BCs on } \Gamma\text{: } \begin{cases} \hat{\mathbf{n}} \times (\mathbf{E}^d + \mathbf{E}_{in}) = 0 \\ \hat{\mathbf{n}} \cdot (\mathbf{B}^d + \mathbf{B}_{in}) = 0 \end{cases} \tag{2.8}$$

It's worth noting that in 2D geometry the so-called s-polarisation (TE polarization) and p-polarisation (TM polarisation) are decoupled, so that under determined conditions they can be treated separately; for s-polarisation we have that the differential problem is given by:

$$\begin{cases} \nabla^2 E_z^d + k^2 E_z^d = 0 & \text{if } y > f(x) \\ E_z^d = -E_{z,in} = -a_z \, E_0 \, e^{ik(x \sin\theta - f(x)\cos\theta)} & \text{if } y = f(x) \end{cases} \tag{2.9}$$

While for p-polarisation:

$$\begin{cases} \nabla^2 B_z^d + k^2 B_z^d = 0 & \text{if } y > f(x) \\ \dfrac{\mathrm{d}B_z^d}{\mathrm{d}n} = -\dfrac{\mathrm{d}B_{z,in}}{\mathrm{d}n} = ib_z k \, E_0 \, (n_y \cos\theta - n_x \sin\theta) e^{ik(x \sin\theta - f(x)\cos\theta)} & \text{if } y = f(x) \end{cases} \tag{2.10}$$

Thus, the condition in order to treat s- and p-polarisation separately is to have:

$$a_z = 1 \Longrightarrow a_x = a_y = b_z = 0 \tag{2.11}$$
$$b_z = 1 \Longrightarrow b_x = b_y = a_z = 0 \tag{2.12}$$

In this way the two cases of polarisation are totally decoupled (actually, in 3D geometry, they form a base of the polarisation vector space). Furthermore, the original vectorial formulation is now reduced to a scalar ones, where the two "fundamental" cases are well decoupled. So, let's analyse these two *scalar diffraction theories*.

2.2 The mathematical problem

From a mathematical point of view the diffraction problem presents many interesting properties. First of all the problem can be formally stated as follows: let F be the analytic function describing the e.m. field in the domain Ω above the grating surface. Then F has to satisfy the Cauchy problem

$$\begin{cases} \nabla^2 F + k^2 F = 0 & \text{in } \Omega \\ F = -g(x) & \text{on } \Gamma \end{cases} \quad \text{or} \quad \begin{cases} \nabla^2 F + k^2 F = 0 & \text{in } \Omega \\ \dfrac{\mathrm{d}F}{\mathrm{d}n} = -\dfrac{\mathrm{d}g(x)}{\mathrm{d}n} & \text{on } \Gamma \end{cases} \tag{2.13}$$

Furthermore, the solution F has to own the symmetries of the geometric configuration. If the equation that F has to satisfy is linear, as in our case, then this means that the spatial expression of the e.m. field has to satisfy the Bloch-Floquet theorem [Floquet 1883]:

$$F(x,y) = e^{ik_x x}\, u(x,y) \qquad \text{where} \quad u(x+d,y) = u(x,y) \tag{2.14}$$

From this we can immediately derive that:

$$F(x+d,y) = e^{ik_x(x+d)}\, u(x+d,y) = e^{ik_x d} e^{ik_x x}\, u(x,y) = e^{ik_x d} F(x,y) \tag{2.15}$$

This can be seen as result of the fact that we are dealing with a discrete translational invariance instead of a continuous one. Thus, our function remains the same only if we jump a distance ℓ that provides a phase shift $k_x \ell = 2\pi n$. For this reason the function F is called "pseudo-periodic".

2.3 The Rayleigh expansion

Since the solution of the scattering problem has to be pseudo-periodic, the reduced function $u(x,y)$ can be expanded in a Fourier series:

$$u(x,y) = \sum_{n=0}^{\infty} u_n(y) e^{inqx} \qquad \text{with} \qquad q = \frac{2\pi}{d} \tag{2.16}$$

so that

$$F(x,y) = \sum_{n=0}^{\infty} u_n(y) e^{i\alpha_n x} \qquad \text{with} \qquad \alpha_n = k_x + nq \tag{2.17}$$

Introducing the pseudo-Fourier expansion of F in the Helmholtz equation gives

$$\sum_{n=0}^{\infty} \left[\frac{du_n}{dy} + (k^2 - \alpha_n^2) u_n \right] e^{inqx} = 0 \tag{2.18}$$

Now, if $y > \max f(x)$, the above equation is valid for any x, and each term of the Fourier series must be zero

$$\frac{du_n}{dy} + (k^2 - \alpha_n^2) u_n = 0 \qquad \forall n \tag{2.19}$$

Defining $\beta_n = \sqrt{k^2 - \alpha_n^2}$ we can write the solution of the above equation as

$$u_n(y) = A_n e^{-i\beta_n y} + B_n e^{i\beta_n y} \qquad \text{if } y > \max f(x) \tag{2.20}$$

The first term, of coefficient A_n, is divergent for $y \to +\infty$ if β_n is imaginary, or represents an incoming plane wave propagating towards the interface. Thus it must hold $A_n = 0 \quad \forall n$ and the diffracted field can be expressed as

$$F(x, y) = \sum_{n=0}^{\infty} B_n e^{i\alpha_n x + i\beta_n y} \qquad \text{if } y > \max f(x) \tag{2.21}$$

This result is very simple and elegant: over the maximums of the modulated surface, the diffracted field can be expressed by the so-called "Rayleigh expansion" from the original work of [Rayleigh 1907], a series of outgoing waves having the same pseudo-periodicity of the interface. It should be noticed that the wave number β_n can be imaginary. In particular, it exists a finite set U for which

$$\beta_n = \begin{cases} \sqrt{k^2 - \alpha_n^2} & \text{if } n \in U \\ i\sqrt{\alpha_n^2 - k^2} & \text{otherwise} \end{cases} \tag{2.22}$$

which means that the *set of outgoing waves is always a finite one.* For these waves the grating formula is valid :

$$\sin\theta_n = \sin\theta + n\frac{\lambda}{d} \tag{2.23}$$

It is worth noting that this formula doesn't depend on the amplitude of the grating nor on its actual shape! It only depends on its period. We can also remark that if we fix the grating period, for increasing wavelength there are orders that "emerge" from evanescence and become propagating. Thus, the number of propagating orders is solely given by the ratio λ/d; furthermore, at the "passing-off" of an order, the energy distribution among the outgoing waves changes suddenly, since more reflecting "channels" become available. This explains why in literature one can find that the energy content of a given order vs. λ shows sudden risings or droppings at particular values of the incident wavelength.
On the other hand we can hardly hope for the grating formula to remain valid for deep gratings too, so we'd better have some "upgraded" theoretical model including the amplitude of the gratings. Different methods for accounting the effect of grating depth will be developed in the next sections, for the moment we insist on the practical use of the grating

formula: in pictures 2.2 is shown the reflection of a normal incidence Gaussian beam from a sinusoidal grating, simulated with our FDTD code (see Appendix A). The parameter of interest are $\lambda = d/2$ and $\theta = 0$, so that according to 2.23 the reflected orders are

$$\begin{cases} n = 0 & \Longrightarrow \quad \theta = 0 \\ n = \pm 1 & \Longrightarrow \quad \theta = \pm\pi/6 \\ n = \pm 2 & \Longrightarrow \quad \theta = \pm\pi/2 \quad \text{! Rayleigh passing-off !} \end{cases} \tag{2.24}$$

that are clearly visible in 2.2b

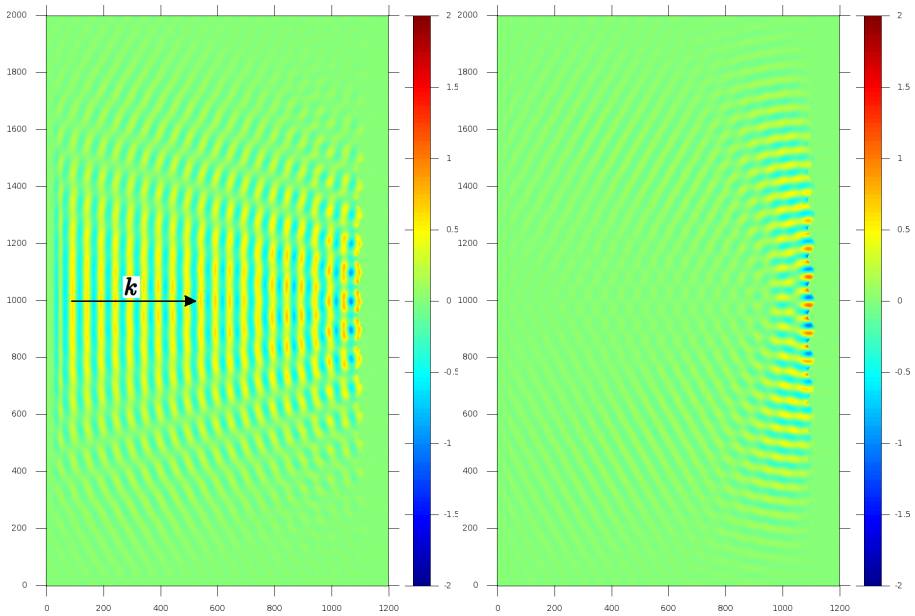

(a) E_y (b) E_x

Figure 2.2: Scattering of a Gaussian beam focused on a sinusoidal grating at normal incidence. The simulation is performed with our FDTD code. The simulation parameters are $\lambda = d/2 = 1\mu m$, $h/d = 0.25$ and beam waist $w_0 = 10\lambda$

2.4 A toy model

In this section we present an ultra-simplified model written by [McDonald] where in the limit of small h/d ratios, the presence of additional reflected waves is a consequence of "perturbed" perfect mirror boundary conditions.
Let's consider a plane wave

$$\mathbf{E}_{in} = E_0 \hat{x} e^{-i(ky+\omega t)} \tag{2.25}$$

impinging normally on a grating defined by

$$y = \frac{h}{2} \sin\left(\frac{2\pi x}{d}\right) \qquad \frac{h}{2d} \ll 1 \tag{2.26}$$

The geometrical sketch of this physical situation is the one depicted in figure 1.1. The electric field is taken along the grating lines; this assumption is necessary since the presence of a preferential direction set by the grating rules, breaks the "degeneracy" between s- and p-polarisation at normal incidence. Thus, even at normal incidence, we distinguish between s-polarisation, when the electric field lies in the invariance direction of the grating (field lines are not bent), and p-polarisation, when the electric field is orthogonal to the grating rules (field lines are bent).
If the (perfectly) conducting surface were flat, the reflected wave would be

$$\mathbf{E}_r = -E_0\hat{x}e^{i(ky-\omega t)} \tag{2.27}$$

However, the sum $E_{in} + E_r$ doesn't satisfy the boundary condition that $\mathbf{E}_{total}$ must be perpendicular to the wavy surface. Indeed,

$$[\mathbf{E}_{in} + \mathbf{E}_r]_{surface} = 2iE_0\hat{x}e^{-i\omega t}\sin(ky_s) \simeq 2i\frac{hk}{2}E_0\hat{x}e^{-i\omega t}\sin(qx) \tag{2.28}$$

where $q = 2\pi/d$ and we have taken $\sin(ky_s) \simeq ky_s = \frac{hk}{2}\sin(qx)$.
Thus, near the surface, there is an additional field that can be decomposed in two waves as follows:

$$\mathbf{E} = hkE_0\hat{x}e^{-i\omega t}\left(e^{iqx} - e^{-iqx}\right) \Longrightarrow \mathbf{E}_\pm = \pm\frac{hk}{2}E_0\hat{x}e^{i(\pm qx-\omega t)} \tag{2.29}$$

Away from the surface, we already know that these new waves can be propagative or evanescent. Then, the full form of the additional waves can be written as

$$\mathbf{E}_\pm = \pm\frac{hk}{2}E_0\hat{x}e^{i(\pm qx+i\kappa y-\omega t)} \tag{2.30}$$

and the constant κ is determined on requiring that each of the additional waves satisfy the wave equation. This leads to the dispersion relation

$$q^2 + \kappa^2 - \frac{\omega^2}{c^2} = 0 \tag{2.31}$$

which can be rewritten as

$$\kappa = 2\pi i\sqrt{\frac{1}{d^2} - \frac{1}{\lambda^2}} \tag{2.32}$$

Thus, the dispersion relation of these waves correspond exactly to the grating formula provided that $n = 1$, i.e. for $\lambda > d$ the waves are evanescent and thus *surface waves*, while in the opposite case they are propagative. It is remarkable that the fact that only the order $n = 1$ come out in this simplified solution is a consequence of retaining only the first order term of the sinus expansion 2.28 in the parameter $hk/2$. Then, the validity condition of the whole method is that both λ and d have to be greater than h, the depth of the grating. We will see in the next section that the condition $h \ll \lambda$ is not necessary to solve the diffraction problem, but in this case it determines the number of evanescent waves that rise from satisfying the boundary conditions. For example, if we want the problem to be accurate at order $O(h^2/d^2)$, we'll have two more additional waves with wave number $\pm 2q$, and so on at increasing order.

Back to mathematics, the evanescent fields now read:

$$\mathbf{E}_{\pm} = \pm\frac{hk}{2}E_0\hat{x}e^{i(\pm qx-\omega t)}\exp\left(-\sqrt{q^2-\frac{\omega^2}{c^2}}\right) \tag{2.33}$$

The model we developed here is a simplified version of the original work performed by [McDonald]. In his work he considered a situation in which the incoming wave enlightens the grating under an angle θ between the light wave vector and the grating rules, which is different from the choice we made in section 2.1 for there the wave vector is orthogonal to the grating rules. Both these choices are particular cases of the more general skew geometry shown in figure 2.3:

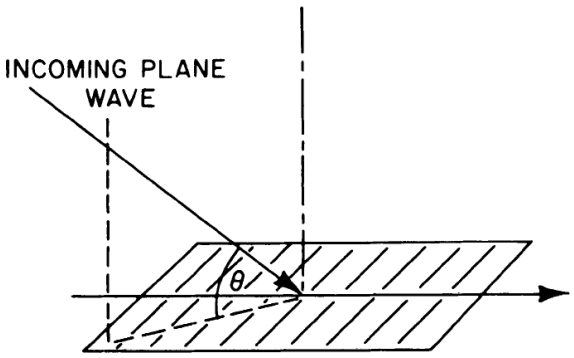

Figure 2.3: Geometric sketch of skew diffraction

Why do they have to take the wave vector in such a direction? We should have said before that the author of this model was studying the diffraction problem in the framework of laser-grating accelerators. As we explained in the introduction, the first attempt to exploit the surface fields for particles acceleration was made by [Takeda 1968] with "our" geometry, i.e. with an azimuthal angle between the wave vector and the grating wave number φ equal to zero. In this situation [Lawson 1979] showed that the acceleration of particles to ultra-relativistic energies is unfavourable, as explained in the following.
We already showed that the diffracted field can be written as a sum of waves of the type:

$$\begin{aligned} E_x &= A_n e^{i\alpha_n x+i\beta_n y-i\omega t} \\ E_y &= \frac{A_n\alpha_n}{\beta_n}e^{i\alpha_n x+i\beta_n y-i\omega t} \qquad \text{where } \beta_n^2 = k^2-\alpha_n^2 \\ E_z &= 0 \quad \text{for p-polarisation} \end{aligned}$$

When $\alpha_n > 1$ the diffracted field is evanescent away from the metal surface and propagates along the grating plane. Thus, in order to accelerate particles along the grating periodicity direction (by the E_x component), the particle speed should match the wave phase velocity (see Chapter 4), so that in its rest frame it feels a constant acceleration. This "surf-like" acceleration is more efficient for ultra-relativistic particles, for which the speed is close to c, since in that case the dephasing associated with the acceleration is much more depressed than in the non-relativistic case.

Thus, since the phase velocity of the surface fields is $v_\phi = \omega/\alpha_n = ck/\alpha_n$, the particle speed should satisfy the condition

$$\alpha_n \beta = k \qquad \text{where } \beta = \frac{u}{c} \tag{2.34}$$

That means that $\beta_n^2 = k^2(1 - 1/\beta^2)$, thus the ratio

$$\frac{E_x}{E_y} = \frac{\beta_n}{\alpha_n}$$

for the mode n approaches zero for ultra-relativistic particles and there can be no further net acceleration. The reason for this is that the only wave consistent with the symmetry condition $dE/dz = 0$ that stays in phase with a particle travelling at the speed of light is a simple propagating plane wave travelling in the direction of the particle. Such a wave is always transversely polarized and thus cannot accelerate in its direction of propagation. In order to overcome this restriction, we have to break the symmetry condition and consider waves travelling at an angle to the beam direction. If, for instance, we simply rotate the incident wave vector by an azimuthal angle $\varphi \in [0, \pi/2]$ with respect to the grating wave number (see fig. 2.3), then the condition 2.34 becomes

$$\alpha_n \beta \cos\varphi = k \qquad \Longrightarrow \qquad \beta_n^2 = k^2(1 - 1/(\beta\cos\varphi)^2) \tag{2.35}$$

Now both β_n and E_x no longer approach zero as β approaches unity, and the effect is at optimum for $\varphi = \pi/2$. That explains the choice of the geometric setting in McDonald example.

2.5 A boundary perturbation method

In section 2.3 we showed how a very simple way of writing the solution of the diffraction problem can be found in the region above the top of the grating grooves. In the previous one instead we found a very rough and effective way of treating the boundary conditions in order to avoid the problem of Rayleigh expansion not being valid in the region within the maxima and minima of the grooves. In this section we derive a rigorous and cumbersome solution based on the effectiveness of the perturbation approach seen above. However the problem is still the same: how can we impose the boundary conditions on the grooves profile if the Rayleigh expansion is not valid within the grooves?
The idea we will follow in this section, which was developed by [Bruno 1993a], is to use a perturbation expansion of the solution of the diffraction problem in a small parameter δ that describe how much the boundary surface is rippled. Use of such a "geometric" perturbation theory is advantageous in the treatment of complex geometries that can be seen as deviations from a simpler one, in this case the reflection from a plane mirror.

2.5.1 Analyticity properties of the electromagnetic field

The perturbation approach bases its validity on a theorem proved by [Bruno 1992] that states the following:

Theorem 2.5.1 (Analyticity of the electro-magnetic field) *Let Ω_δ be a family of boundaries described by the function $\mathbf{r}_s = H(s,\delta)$, where H is jointly analytic in the curvilinear abscissa s and expansion parameter δ. Then it holds:*

- ▷ *$F(\mathbf{r},\delta)$ is jointly analytic in the parameters $(\mathbf{r},\delta)$*
- ▷ *$F(\mathbf{r_s},\delta)$ is analytic in the parameter δ*

This mean that the field in the upper space and on the grating surface changes smoothly with boundary variations. The usefulness of this apparently obvious result will be clear in the next section.

2.5.2 Recursive formulas

Since the field F is analytic with respect to boundary perturbation, we can expand it in Taylor series

$$F(x,y,\delta) = \sum_{n=0}^{\infty} F_n(x,y)\,\delta^n \qquad \text{with} \qquad F_n \equiv \frac{1}{n!}\left.\frac{\partial^n F}{\partial \delta^n}\right|_{\delta=0} \tag{2.36}$$

Inserting the above expansion in the Helmholtz equation we notice that the set of F_n components satisfy the same linear problem as before:

$$\nabla^2 F_n + k^2 F_n = 0 \qquad \text{in } \Omega_0 = \{(x,y)|y>0\} \tag{2.37}$$

so that also every F_n can be expressed by means of Rayleigh expansion:

$$F_n(x,y) = \sum_r d_{n,r} e^{(i\alpha_r x + i\beta_r y)}\,\delta^n \tag{2.38}$$

It's worth noticing that for F_n the validity hypothesis of Rayleigh expansion leads us to affirm that such expansion holds for any (x,y) in Ω_0, since there's no groove now!
Furthermore, from 2.21, we have

$$F(x,y,\delta) = \sum_r B_r(\delta) e^{(i\alpha_r x + i\beta_r y)}$$

we can identify

$$B_r(\delta) = \sum_{n=0}^{\infty} d_{n,r}\delta^n \qquad \Longleftrightarrow \qquad d_{n,r} = \frac{1}{n!}\left.\frac{d^n B_r}{d\delta^n}\right|_{\delta=0} \tag{2.39}$$

What we have to do now is to compute the coefficients $\{d_{n,r}\}$. In order to achieve is we have to impose the boundary conditions and carry out the rather cumbersome calculations the details of which are given in Appendix B. The result is the following formulae:

S-polarisation:

$$d_{n,r} = -(-ik_y)^n C_{n,r} - \sum_{\ell=0}^{n-1} \sum_{\kappa=\max\{-\ell S, r-(n-\ell)S\}}^{\min\{\ell S, r+(n-\ell)S\}} C_{n-\ell,r-\kappa}(i\beta_\kappa)^{n-\ell} d_{\ell,\kappa} \tag{2.40}$$

P-polarisation:

$$i\beta_r d_{n,r} = (-ik_y)^{n-1}(k_y^2 - k_x rq)C_{n,r} + \\ + \sum_{\ell=0}^{n-1} \sum_{\kappa=\max\{-\ell S, r-(n-\ell)S\}}^{\min\{\ell S, r+(n-\ell)S\}} C_{n-\ell,r-\kappa}(i\beta_\kappa)^{n-\ell-1}\left[\beta_\kappa^2 - \alpha_\kappa(r-\kappa)q\right] d_{\ell,\kappa} \tag{2.41}$$

where $C_{n,r}$ are the Fourier coefficients of the function defined as:

$$f(x) = \sum_{r=-S}^{S} C_r e^{irqx} \quad \Longrightarrow \quad \frac{f^n}{n!} = \sum_{r=-nS}^{nS} C_{n,r}\, e^{irqx} \tag{2.42}$$

2.5.3 How to use the recursive formulae: application to sinusoidal interfaces

Let's assume again that the interface profile is given by

$$f(x) = \frac{h}{2}\cos(qx) \tag{2.43}$$

so that the expansion parameter is $\delta = h/2$ (the depth of the grooves), which have to be small compared to d, the periodicity of the grooves. The coefficients $C_{r,n}$ for the selected interface function are:

$$C_{n,r} = \begin{cases} \begin{pmatrix} n \\ \frac{n-r}{2} \end{pmatrix} & \text{if } n-r \text{ is even} \\ 0 & \text{if } n-r \text{ is odd} \end{cases} \tag{2.44}$$

Furthermore, for the sake of simplicity let be at normal incidence, $\theta = 0$, so that

$$\beta_r = \sqrt{k^2 - r^2 q^2} \tag{2.45}$$

Thus the condition to have waves reflected away form the surface is $r\frac{\lambda}{d} > 1$, so if for example we set $\lambda/d = 0,45$ the set of diffracted waves is given by

$$U = \{0, \pm 1, \pm 2\}$$

in agreement with the grating formula 2.23.
The first right hand member of equation B.8 tell us that if, as in our case, $S = 1$, then $|r| \leqslant n$. Considered from the opposite point view, this means that the order $r = \pm 3$, that in our case is the first evanescent order, appears as power of δ of order $n \geqslant 3$. That's to say that $B_3(\delta) = O(\delta^3)$, and, generally speaking

$$B_{\bar{r}}(\delta) = O(\delta^{\bar{r}}) \tag{2.46}$$

As counter proof of what's been just stated, let's think to the limit in which $\delta \to 0$. We can image this as d becoming much bigger than h. If we keep the h/λ ratio fixed, we

notice by equation 2.23 that the number of diffracted waves keeps rising as well as the spacing between the wavevectors keeps falling. As soon as $\lambda/d \to 0$ equation 2 reads

$$\sin\theta_n = \sin\theta \qquad \forall n$$

That's when the diffraction grating is a plane mirror, and we know that in this situation there's no evanescent wave on the vacuum (air) side.

So, if we assume the simpler case in which $\lambda > d$ then the only radiative order is B_0, and we expect that the evanescent field will be of order δ. That's actually the case of s-polarisation: starting from $d_{0,0} = -1$ and noticing that from the above selection rules $d_{1,0} = 0$, we have

$$d_{1,\pm1} = ikC_{1,\pm1} - C_{1,\pm1}(i\beta_0)d_{0,0} = 2ikC_{1,\pm1} \tag{2.47}$$

Since $C_{1,\pm1} = 1/2$ our evanescent waves become:

$$E_{\pm}^{(1)} = ik\delta\,\exp\left(i\alpha_{\pm1}x + i\beta_{\pm1}y - i\omega t\right) = i\frac{hk}{2}\,e^{\pm iqx - i\omega t}\exp\left(-\sqrt{q^2-k^2}\right) \tag{2.48}$$

that is exactly the same solution found with the simple model derived by McDonald in section 2.4.

2.6 Chandezon technique

Another way to solve the diffraction problem, and perhaps the most natural one, is to shift the difficulty of the analysis from the boundary conditions to the equations themselves. There is a technique first developed by [J. Chandezon 1982] that consists in solving Maxwell equations in a coordinates system where the modulated interface is flat. The price (there is always a price) is that Maxwell equations become more cumbersome. On the other hand this method is valid also for dielectric or metallic materials, where their optical properties can be described by the introduction of a dielectric constant ε.

2.6.1 Change of coordinates system

Let's perform a coordinates change given by:

$$\begin{cases} v &= x \\ u &= y - s(x) \end{cases} \tag{2.49}$$

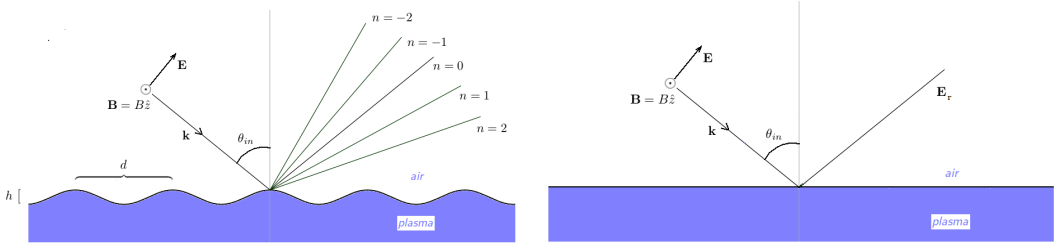

(a) *Original space* (b) *Transformed space*

Figure 2.4: Change of reference frame: from the Cartesian system where the metallic interface is modulated, we move to another reference where the surface is flat. This makes it easier to deal with the boundary condition, at the price of a more complex differential system

The Jacobian of the transformation is

$$\mathcal{J} = \begin{pmatrix} \frac{\partial v}{\partial x} & \frac{\partial v}{\partial y} \\ \frac{\partial u}{\partial x} & \frac{\partial u}{\partial y} \end{pmatrix} = \begin{pmatrix} 1 & 0 \\ -s'(x) & 1 \end{pmatrix} \tag{2.50}$$

How do the derivative operators transform? By the chain rule we get:

$$\begin{cases} \frac{\partial}{\partial x} &= \frac{\partial v}{\partial x}\frac{\partial}{\partial v} + \frac{\partial u}{\partial x}\frac{\partial}{\partial u} = \frac{\partial}{\partial v} - s'\frac{\partial}{\partial u} \\ \frac{\partial}{\partial y} &= \frac{\partial v}{\partial y}\frac{\partial}{\partial v} + \frac{\partial u}{\partial y}\frac{\partial}{\partial u} = \frac{\partial}{\partial u} \end{cases} \implies \begin{pmatrix} \partial_x \\ \partial_y \end{pmatrix} = \begin{pmatrix} 1 & -s' \\ 0 & 1 \end{pmatrix} \begin{pmatrix} \partial_v \\ \partial_u \end{pmatrix} \tag{2.51}$$

Thus:

$$\nabla_{v,u} = (\mathcal{J}^t)^{-1}\nabla_{x,y} \tag{2.52}$$

Since we know that the gradient is a covariant vector, the way derivatives transform show us how the electromagnetic fields themselves transform [R. Dusseaux 1995]:

$$\begin{cases} \mathbf{E},\, \mathbf{H} & : \text{ convariants} \\ \mathbf{B},\, \mathbf{D} & : \text{ contravariants} \end{cases} \implies \begin{cases} \mathbf{E}' = (\mathcal{J}^t)^{-1}\mathbf{E}, & \mathbf{H}' = (\mathcal{J}^t)^{-1}\mathbf{H} \\ \mathbf{B}' = \mathcal{J}^t\mathbf{B}, & \mathbf{D}' = \mathcal{J}^t\mathbf{D} \end{cases} \tag{2.53}$$

2.6.2 Maxwell equations as an eigenvalue problem

With these substitutions, Ampère and Faraday laws can be rewritten as:

$$\frac{\partial F}{\partial u} = \frac{s'(x)}{1+s'(x)^2}\frac{\partial F}{\partial x} - i\frac{1}{1+s'(x)^2}G \tag{2.54}$$

$$\frac{\partial G}{\partial u} = -i\frac{\partial}{\partial x}\left(\frac{1}{1+s'(x)^2}\frac{\partial F}{\partial x}\right) - ik^2F + \frac{\partial}{\partial x}\left(\frac{s'(x)}{1+s'(x)^2}G\right) \tag{2.55}$$

where

$$\begin{cases} \left.\begin{array}{l} F = E_z(x,u) \\ G = kH_x(x,u) \end{array}\right\} & \text{for s-polarisation} \\ \left.\begin{array}{l} F = H_z(x,u) \\ G = -\varepsilon k E_x(x,u) \end{array}\right\} & \text{for p-polarisation} \end{cases} \tag{2.56}$$

If we introduce the quantities:

$$c(x) = \frac{1}{1+s'(x)^2}, \quad d(x) = \frac{s'(x)}{1+s'(x)^2}, \quad \psi = \begin{pmatrix} F \\ G \end{pmatrix}$$

our differential system takes the elegant form

$$i\frac{\partial \psi}{\partial u} = \mathcal{L}\psi \tag{2.57}$$

where the differential operator is defined as

$$\mathcal{L} = \begin{pmatrix} id(x)\frac{\partial}{\partial x} & c(x) \\ \frac{\partial}{\partial x}\left[c(x)\frac{\partial}{\partial x}\right] + k^2 & i\frac{\partial}{\partial x}d(x) \end{pmatrix} \tag{2.58}$$

Now, recalling that our e.m. field has to be pseudo-periodic, we can expand the function ψ in

$$\psi = \sum_m \psi_m(u) e^{i\alpha_m x} \qquad \text{where } \alpha_m = k_\parallel + mq \tag{2.59}$$

and similarly

$$c(x) = \sum_n c_n e^{inqx} \tag{2.60}$$

$$d(x) = \sum_n d_n e^{inqx} \tag{2.61}$$

Thus, the problem may be rewritten as

$$-i\frac{\partial F_m}{\partial u} = \sum_n \left[\alpha_n d_{m-n} F_n + c_{m-n} G_n\right] \tag{2.62}$$

$$-i\frac{\partial G_m}{\partial u} = \sum_n \left[(-\alpha_m \alpha_n c_{m-n} + \varepsilon k^2) F_n + \alpha_m d_{m-n} G_n\right] \tag{2.63}$$

or

$$-i\frac{d\xi(u)}{du} = \mathbb{T}\xi(u) \tag{2.64}$$

where $\xi(u) = (F_1, \dots, F_m, \dots, G_1, \dots, G_m, \dots)$ and matrix $\mathbb{T}$ is given by

$$\mathbb{T} = \begin{pmatrix} \mathbb{A} & \mathbb{B} \\ \mathbb{C} & \mathbb{D} \end{pmatrix} \qquad \text{where} \begin{cases} A_{mn} &= \alpha_n d_{m-n} \\ B_{mn} &= c_{m-n} \\ C_{mn} &= -\alpha_m \alpha_n c_{m-n} + \varepsilon k^2 \delta_{mn} \\ D_{mn} &= \alpha_m d_{m-n} \end{cases} \tag{2.65}$$

This can be readily solved as an infinite dimensional eigenvalue problem searching for solutions of the kind

$$\xi_j(u) = \phi_j e^{i\lambda_j u} \quad \Longrightarrow \quad \xi(u) = \sum_q a_j \phi_j e^{i\lambda_j u} \tag{2.66}$$

where $\{\lambda_j\}$ is the set of eigenvalues and $\{\phi_j\}$ the set of eigenvectors.
As final remark we'd like to point out that back in our original coordinates the solution of the problem, for example in p-polarisation, read:

$$H(x,y) = \sum_m \sum_j F_{mj} \underbrace{\exp[i\lambda_j(y - s(x))]}_{\neq \text{ Rayleigh's expansion}} \exp(i(k_x + mq)x) \tag{2.67}$$

As one may notice, the expression in brace in formula 2.67 is what differs from the Rayleigh's expansion, which now is valid for every periodic boundary shape whose expression can be taken in the form

$$y_s = s(x)$$

.

Chapter 3

Surface plasmon resonance

The perturbation method derived in section 2.5 can be generalized to dielectric and metallic grating, which are of common use both in theory and in experiments.

However, in order to obtain high precision results, one have to choose a proper truncation of the series 2.39.

Use of the method of Padé approximants as in [Bruno 1993b] in the case of dielectric grating (with index of refraction n = 2) leads for example to

s-polarisation	R	T	err $= 1-(R+T)$
$h = 0.2$	0.117282	0.882718	$< 10^{-7}$
$h = 0.5$	0.055902	0.944098	10^{-7}
p-polarisation			
$h = 0.2$	0.086355	0.913645	$< 10^{-7}$
$h = 0.5$	0.025636	0.974363	$7{\cdot}10^{-7}$

Comparison with our FTDT simulation with grating depths $h = 0.2$ and $h = 0.5$ performed on a broad range of wavelengths gives for the correspondent λ/d ratios:

s-polarisation	R	T	err $= 1-(R+T)$
$h = 0.2$	0.117	0.881	$2{\cdot}10^{-3}$
$h = 0.5$	0.057	0.937	$6{\cdot}10^{-3}$
p-polarisation			
$h = 0.2$	0.0892	0.9112	$-7{\cdot}10^{-4}$
$h = 0.5$	0.02734	0.97264	$2.{\cdot}10^{-5}$

that shows a very good agreement among the collected results.

These results were obtained by computing the reflectivity spectrum of a broadband e.m. pulse normally incident on a sinusoidal grating. For details of the numerical technique employed by our code, see Appendix A.

On the other hand, if we compute the spectral response of a metallic grating (*non-* perfect conductor) with the same simulation code, we get as reflection spectrum what is shown in figures 3.1:

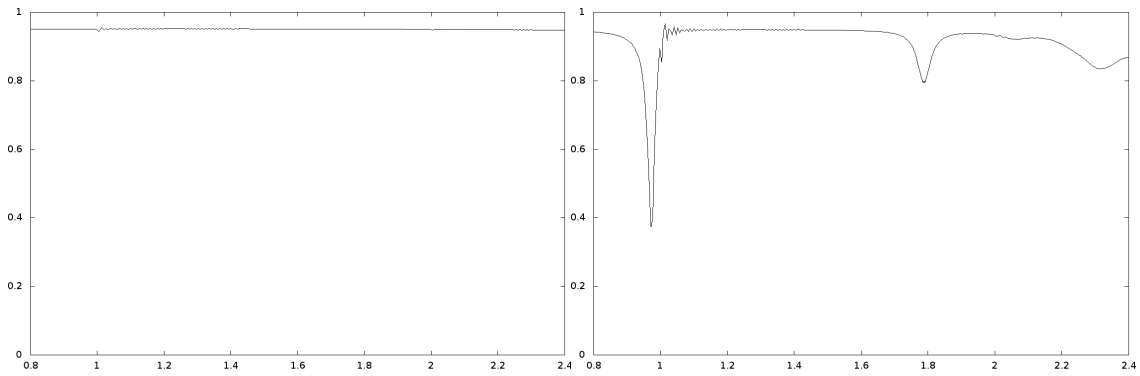

(a) *s-polarisation* (b) *p-polarisation*

Figure 3.1: Simulation of the Reflectivity spectrum of s- and p-polarised light normally incident on a diffraction grating with our FDTD code. While for most frequencies of the incident light the grating behaves like a mirror, for given frequencies the reflectivity coefficient drops to much lower values. Since no transmission occurs, the "missing" light has to be confined near the surface, revealing the presence of a new surface phenomenon. The simulation parameters are: Grating depth $h = 0.1\mu m$, Grating pitch $d = 1\mu m$, Normalized plasma frequency $\omega_p^2/\omega_0^2 = 25$, with $\omega_0 = 2\pi c/d$ the normalizing frequency

While in s-polarisation all the incident light is reflected back as in a flat mirror reflection, that's no longer the case in p-polarisation, where a set of *resonant frequency* appear and have values that turn out to be unpredictable with the models derived in the previous chapter. This means that in p-polarisation, modelling our diffraction grating as made of a perfectly conductive material is *wrong*! We have to take into account that the metal the grating is made of, has a finite negative real dielectric constant and that absorption may occur due to a series of electronic phenomena occurring at the surface. Therefore, in the following we will model our grating as made of metal, with optical properties described by a Drude dielectric constant:

$$\epsilon(\omega) = 1 - \frac{\omega_p^2}{\omega(\omega + i\nu)} \qquad \text{where } \omega_p^2 = \frac{4\pi e^2 n_e}{m_e} \tag{3.1}$$

and ν takes into account the possible lossy phenomena that may happen during the reflection process.
The failure of the PEC (Perfect Electric Conductor) model in predicting these "negative resonances" in the reflectivity spectrum was first pointed out by Maystre in 1972 [Maystre 1984], which formulated a rigorous integral theory of scattering from grating that we do not report here.
We will see in this section that the word "resonance" is not misused, since it will be shown that those sinks in the reflectivity coefficient correspond to poles in the Fresnel formulas for reflection and transmission. From a mathematical point of view this is related to the fact that the system we are studying owns a certain number of *eigenmodes* that can be resonantly excited by satisfying a given matching condition. Thus, as in any eigenvalue problems, we can investigate the existence of eigenmodes, which in our case are solutions

of Maxwell's equation, and their dispersion relation (the infinite set of solutions of the characteristic polynomial). From a physical point of view we can imagine that, given an external source that matches our eigenmode, the reflected and transmitted fields are much greater than the incident field, i.e. they correspond to a pole in the reflectivity coefficient. How is this possible without violating the energy conservation relation? The answer is in the next paragraph.

3.1 Fresnel coefficients in the complex domain

Let a p-polarized plane wave of wavelength k imping on a flat mirror with an incidence angle θ:

$$\begin{cases} B(x,y) = e^{ik(\alpha x - \beta y)} + r(\alpha)e^{ik(\alpha x + \beta y)} & \text{for } y > 0 \\ B(x,y) = t(\alpha)e^{ik(\alpha x - \gamma y)} & \text{for } y < 0 \end{cases} \tag{3.2}$$

where $\alpha = \sin\theta$, $\beta = \cos\theta = \sqrt{1-\alpha^2}$ and $\gamma = \sqrt{\mathrm{n}^2 - \alpha^2}$. Then the Fresnel coefficients are given by [Born 1999]:

$$r(\alpha) = \frac{\mathrm{n}^2\beta - \gamma}{\mathrm{n}^2\beta + \gamma} \qquad t = \frac{2\mathrm{n}^2\beta}{\mathrm{n}^2\beta + \gamma} \tag{3.3}$$

Thus, if we are dealing with a dielectric mirror, $\mathrm{n}^2 > 0$ and the denominators of equations 3.3 never go to zero (Here an interesting phenomenon occurs when $r(\alpha) = 0$, with α given by the Brewster formula). On the other hand, if we replace our dielectric material with a metallic one, and we assume for the sake of clarity $\mathrm{n}^2 = \epsilon_r$ to be real, then $\mathrm{n}^2 < 0$ and γ becomes purely imaginary. This means that we have to define the Fresnel coefficients in the complex domain, and look for singular points. It turns out that the condition $\mathrm{n}^2\beta + \gamma = 0$ is fulfilled by

$$\hat{\alpha}_{plane} = \frac{\mathrm{n}}{\sqrt{1+\mathrm{n}^2}} \tag{3.4}$$

It is interesting to observe that the same result does not hold for the s-polarisation case since there the Fresnel coefficient would read:

$$r(\alpha) = \frac{\beta - \gamma}{\beta + \gamma} \qquad t = \frac{2\beta}{\beta + \gamma} \tag{3.5}$$

thus no pole in the denominator of r can be found even for imaginary refractive indexes. Its physical explanation is very similar to that of the well known phenomenon of resonant absorption (see for a correct description [Hinkel-Lipsker 1991]): the resonant feature of the surface mode is due to the collective excitation of electrons in proximity of the metal surface. In order for this "polarization" of the material to occur, one has to externally drive it with an electric field component *which lies in the plane of incidence*. Thus only for p-polarised light there is the so-called "surface plasmon-polariton resonance".
For completeness we should argue that if the metal we are considering is magneto-active and in particular with negative diamagnetic constant μ then according to the more general Fresnel coefficients

$$r_s(\alpha) = \frac{\mu\beta - \gamma}{\mu\beta + \gamma} \qquad r_p(\alpha) = \frac{\epsilon\beta - \mu\gamma}{\epsilon\beta + \mu\gamma} \tag{3.6}$$

it can exists a "magnetic plasmon" which can be excited only in s-polarisation! This kind of materials are called "meta-materials" and despite not existing in nature, they can be artificially synthesized and used in optics to manipulate optical paths in awesome ways. For the first theoretical study of meta-materials, see [Veselago 1968].
Back to our problem it shall be noticed that

$$\begin{cases} \text{if} \quad \mathrm{n}^2 < -1 & \Longrightarrow \quad \hat{\alpha}_{plane} = \dfrac{\mathrm{i}\tilde{\mathrm{n}}}{\mathrm{i}\sqrt{\tilde{\mathrm{n}}^2 - 1}} > 1 \\ \text{if} \quad -1 < \mathrm{n}^2 < 0 & \Longrightarrow \quad \hat{\alpha}_{plane} = \dfrac{\mathrm{i}\tilde{\mathrm{n}}}{\sqrt{1 - \tilde{\mathrm{n}}^2}} \in \Im \end{cases} \tag{3.7}$$

Using the parameters of simulation 3.1b we get n = 4.90i, so our propagation constants are:

$$\hat{\alpha}_{plane} = 1.02 \tag{3.8}$$

$$\hat{\beta}_{plane} = 0.21\mathrm{i} \tag{3.9}$$

$$\hat{\gamma}_{plane} = 5.00\mathrm{i} \tag{3.10}$$

It is evident that this kind of "propagation coefficient" doesn't represent a propagative wave. They describe a wave propagating parallel to the mirror surface but which is *evanescent* in the orthogonal direction! The resonant mode just found is confined near the discontinuity interface, and its energy depends on the coupling mechanism with an external source. Furthermore, the evanescent feature of this surface mode explains the presence of sinks in the p-polarisation reflectivity spectrum: when the excitation of a surface mode occurs, we observe a fall of the reflected field due to its confinement near the discontinuity interface.
On the other hand, such a resonance could never be excited by an incident plane wave, since both $\alpha = \sin\theta$ and $\beta = \cos\theta$ are always real and smaller than 1, so that no "matching" with the wavevectors in 3.8 could be achieved. That's the reason why a series of techniques to ensure the possibility of excitation of these modes have been developed and are of common use in the field of plasmonics (See for example [Maier 2007]).

3.2 Fresnel coefficients & diffraction gratings

A common method used to excite surface plasmon resonances is to introduce a periodic modulation on the discontinuity surface between metal and air (dielectric). In this configuration we already know that the total field can be written as the sum of an incidence and a scattered field:

$$\begin{cases} B(x,y) = e^{ik(\alpha x - \beta y)} + \displaystyle\sum_n B_n\, e^{ik(\alpha_n x + \beta_n y)} & \text{for } y > h/2 \\ B(x,y) = \displaystyle\sum_n C_n e^{ik(\alpha_n x - \gamma_n y)} & \text{for } y < -h/2 \end{cases} \tag{3.11}$$

with $\alpha_n = \alpha + n\lambda/d$ and β_n, γ_n defined as before.
Then, if for the sake of simplicity we suppose that the 0-order is the only propagative order of reflection our α_ns are placed in the complex plane as shown in figure 3.2:

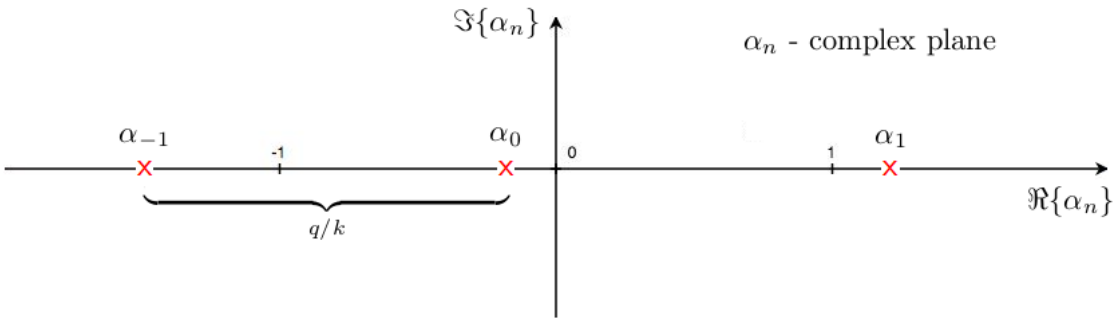

Figure 3.2: Complex plane of α_n *coefficients*

Now, if we want our reflected field to be a resonant one, we shall be able to express equation 3.11 as:

$$B(x,y) = \sum_n \hat{B}_n \, e^{ik(\hat{\alpha}_n x + \hat{\beta}_n y)} \tag{3.12}$$

i.e. the incident field should be negligible in comparison with the reflected part.
Since this expansion is valid only above the maxima of the grooves, we can link the coefficients in the above equation with $\hat{\alpha}_{plane}$ by exploiting the analyticity properties of the electromagnetic field given in section 2.5.1, i.e. the resonant field on a diffraction grating must tend, as soon as h goes to zero, to the resonant field on the plane mirror. Thus, recalling that each B_n is of order δ^n, since $\hat{\alpha}_{plane}$ is greater than unity, we can state that up to leading order:

$$\lim_{h\to 0} \hat{\alpha}_1 = \hat{\alpha}_{plane} \tag{3.13}$$

while the other coefficients go to zero. This allow us to discard the infinite set of poles of the Fresnel coefficient but the leading order term.
This result is of extremely useful because, if we guess that it still holds for mildly deep gratings, it allows us to identify as responsible for the reflectivity sinks the first evanescent mode after the passing-off. From the opposite point of view, if we know the dispersion relation for the surface mode, we will be able to compute the frequency associated to the pole we're studying and therefore predict the position of a sink in the reflectivity spectrum.

3.3 Electromagnetic surface modes

It should be noticed that the mathematical results of diverging reflected and transmitted fields, even if they're localized in proximity of the interface and thus not violating any radiation conditions, has no physical meaning. A more correct point of view consists in saying that we can have finite amplitude reflected and transmitted fields with no incident

field at all. Back to mathematical language, this means that the system with are investigated owns a certain amount of eigenmodes, that can be computed by linear algebra techniques.
In order to derive the surface mode dispersion relation we have to look for a non-trivial solution of the *homogeneous* Maxwell's equations in presence of a flat discontinuity surface and later add a modulation to the surface and see what happens. Bearing in mind that the field we are describing has to be p-polarized and evanescent in the direction orthogonal to the interface, we can suppose our $\mathbf{B} = B(x, y)\mathbf{z}$ to be given by:

$$B(x, y) = Ae^{i(k_{sp}y-\omega t)} \left[e^{-\kappa_m x}\vartheta(x) + e^{\kappa_a x}\vartheta(-x)\right] \tag{3.14}$$

where $\vartheta(x)$ is the Heavyside function and κ_m, κ_a are the inverse evanescence lengths in the metal and in air.
This field has to satisfy the wave equation:

$$\nabla \times \nabla \times \mathbf{B} - \epsilon_i \frac{\omega^2}{c^2}\mathbf{B} = 0 \qquad \text{with } i = m, a \tag{3.15}$$

that leads to

$$-\nabla^2\mathbf{B} - \epsilon_i \frac{\omega^2}{c^2}\mathbf{B} = 0 \qquad \text{with } i = m, a \tag{3.16}$$

in both materials for $y \neq 0$. Substitution of expression 3.14 in the above equation gives

$$-k_{sp}^2 + \kappa_i^2 + \epsilon_i \frac{\omega^2}{c^2} = 0 \quad \Longrightarrow \quad \begin{cases} \kappa_a = \sqrt{k_{sp}^2 - \dfrac{\omega^2}{c^2}} & \text{for } x < 0 \\ \kappa_m = \sqrt{k_{sp}^2 - \epsilon\dfrac{\omega^2}{c^2}} & \text{for } x > 0 \end{cases} \tag{3.17}$$

What we shall further require is the continuity of the electric field parallel to the interface. So according to the p-polarization set of equations 2.8, the permorming of x-derivative of the field given in 3.14 leads to

$$-\frac{\kappa_m}{\varepsilon_m} = \frac{\kappa_a}{\varepsilon_a} \qquad \Longrightarrow \qquad \frac{\kappa_m}{\kappa_a} = -\varepsilon \tag{3.18}$$

Thus dividing side by side the expression in parentheses of equation 3.17 and carrying out the algebra we finally obtain the surface plasmon dispersion relation:

$$k_{sp}^2 = \frac{\omega^2}{c^2}\frac{\varepsilon}{1+\varepsilon} \quad \Longrightarrow \quad \underbrace{k_{sp}^2 = \frac{\omega^2}{c^2}\left(\frac{\omega^2 - \omega_p^2}{2\omega^2 - \omega_p^2}\right)}_{\text{for a Drude metal}} \tag{3.19}$$

The dispersion curve is shown in figure 3.3:

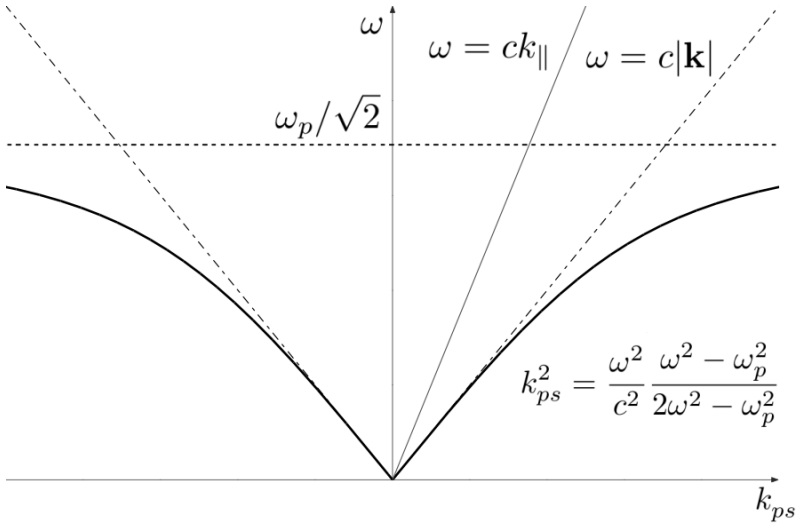

Figure 3.3: Dispersion relation for a surface plasmon on a Drude metal

The graph of the dispersion relation is useful to visualize a possible matching condition. In the case of light scattering from a flat metallic interface no matching condition can be found, as expected from discussion in the previous section. In fact, conservation of momentum along the y direction gives the matching condition $k_{sp} = k_{\parallel} = k \sin\theta$, which causes no intersection between the light and plasmon curves to occur.

On the contrary, if we have a diffraction grating, the momentum condition becomes:

$$k_{sp} = k_{\parallel} \pm nq \qquad \text{with } q = \frac{2\pi}{d} \tag{3.20}$$

If we substitute this relation in equation 3.19 we find that the graph of the new dispersion relation contains a discrete (and infinite) set of *alias* of the original curve, each one displaced along the k_{sp} axis by a quantity equal to $\pm nq$. So, following the usual procedure well known to any solid state physicists (see for example [Ashcroft 1976]), we can restrict our domain of investigation in the momentum space to the first Brillouin zone

$$k_{sp} \in \left[-\frac{q}{2}, \frac{q}{2}\right]$$

and fold back our plasmon dispersion graph as soon as k_{sp} approaches a half Bragg's vector, as shown in the figures 3.6:

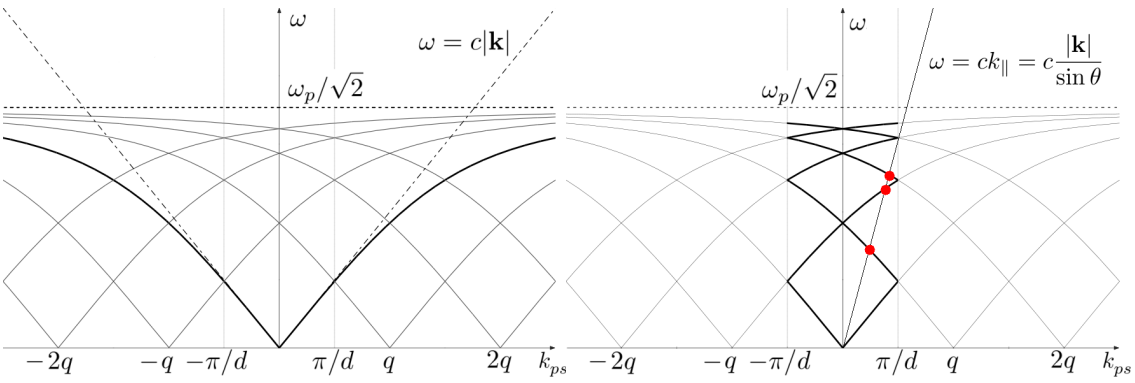

(a) *curve replicas* (b) *Bragg reflection*

Figure 3.4: Construction of First Brillouin Zone. In figure on the right, the light curve intersect the plasmon dispersion relation an infinite number of times. It should be notice that also the light curve itself is fold back into the first Brillouin zone by the grating periodicity

With such a construction we are now able to explain the presence of sinks in the spectrum shown in figure 3.1b. If we set $\theta = 0$ (i.e. normal incidence) and we let the frequency vary, we expect to find in a reflectivity spectrum as many plasmon resonances as the number of intersection between the plasmon curve and the ω axis. The formula for the solutions of this intersection is

$$\omega_n^2 = \frac{\omega_p^2}{2} + n^2q^2c^2 - \sqrt{\frac{\omega_p^4}{4} + n^4q^4c^4} \tag{3.21}$$

which are shown graphically in figure 3.5:

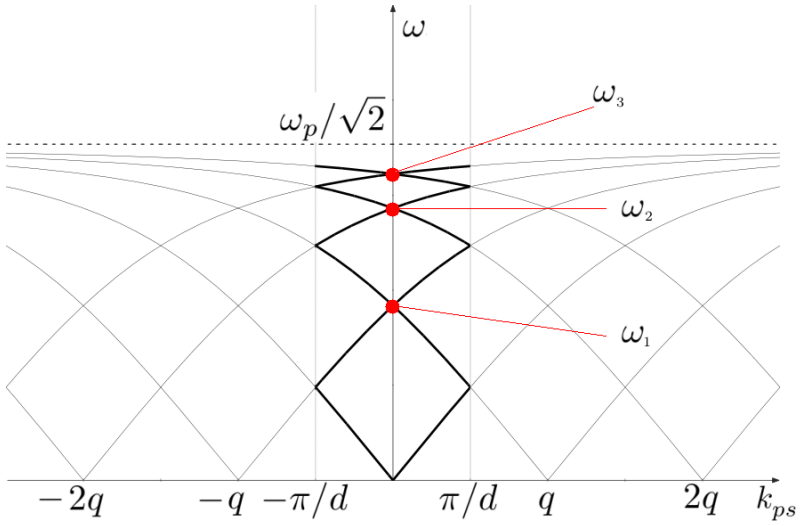

Figure 3.5: Graphic solution of plasmon-photon coupling at normal incidence

If we retrieve the parameters used to obtain simulation 3.1b, i.e. $d = \lambda_0$, $\omega_0 = 2\pi c/\lambda_0$, $\omega_p^2/\omega_0^2 = 25$ and we normalize the above equation to ω_0^2, we obtain from the dimensionless

relation

$$\frac{\omega_n^2}{\omega_0^2} = \frac{n_e}{2n_{cr}} + n^2\frac{\lambda_0^2}{d^2} - \sqrt{\frac{n_e^2}{4n_{cr}} + n^4\frac{\lambda_0^4}{d^4}}$$

that the first three resonances should be located at

$$\tilde{\omega}_1 = 0.9799, \quad \tilde{\omega}_2 = 1.8373, \quad \tilde{\omega}_3 = 2.4692$$

that's in really good agreement with the position of the sinks obtained in the simulations shown below:

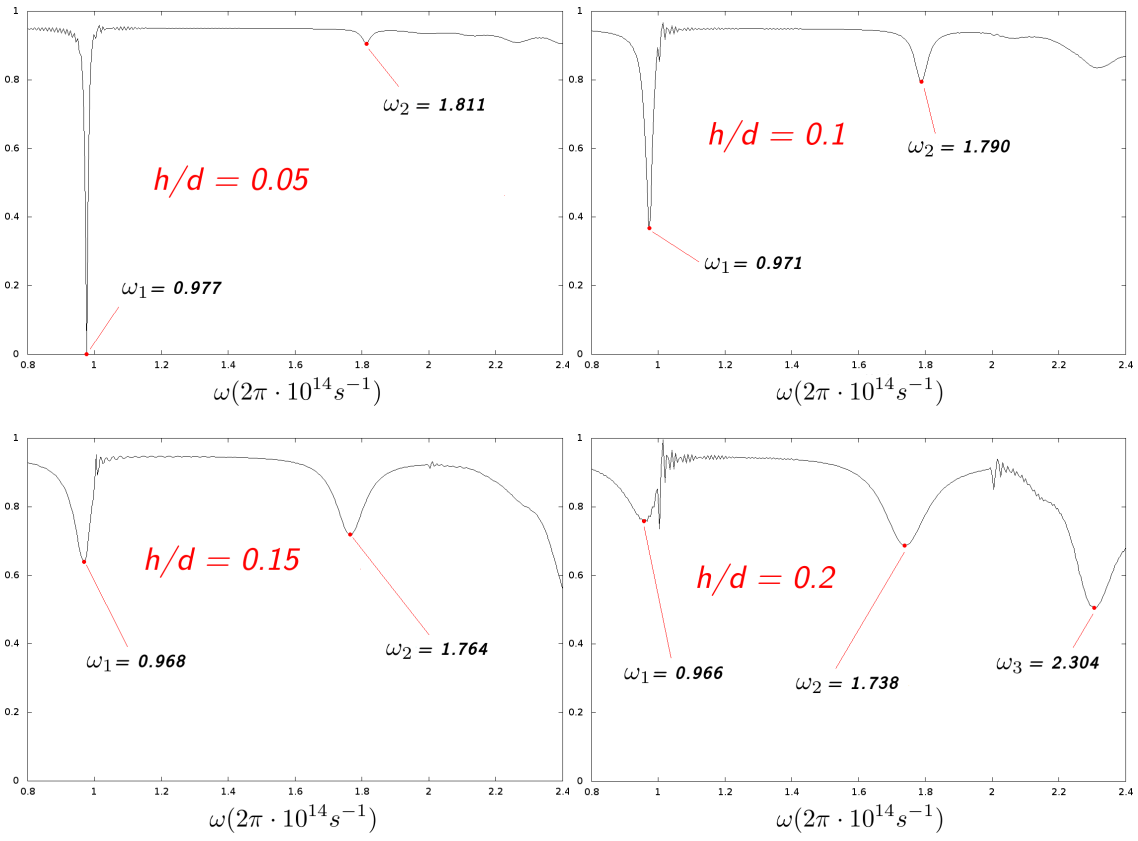

Figure 3.6: Position of resonant frequancies at increasing h/d

We may wonder why we observe a "red shift" of the resonant frequencies in correspondence with an increase in the h/d ratio. The reason is that in our simple model we have totally neglected the interaction among different harmonics of q that can rise or lower the energy content of each resonant mode. More intuitively, we have simply folded our dispersion relation into the FBZ without worrying about the possibility for the dispersion curve itself to be modified by the fact that the small amplitude of the grooves actually is not so small. In the next section we will derive a way to take into account the effects of the h/d parameter.

3.4 Red shift of resonant frequencies

It must be noticed that at normal incidence, the resonant frequency presents a degeneracy which can be removed considering the interaction between the two modes involved. To do so analytically the Chandezon technique presented in the previous chapter proves to be extremely useful. In fact, if we look at matrix $\mathbb{T}$, that we report here:

$$\mathbb{T} = \begin{pmatrix} \mathbb{A} & \mathbb{B} \\ \mathbb{C} & \mathbb{D} \end{pmatrix} \qquad \text{where} \begin{cases} A_{mn} &= \alpha_n d_{m-n} \\ B_{mn} &= c_{m-n} \\ C_{mn} &= -\alpha_m \alpha_n c_{m-n} + \varepsilon k^2 \delta_{mn} \\ D_{mn} &= \alpha_m d_{m-n} \end{cases} \tag{3.22}$$

we realize that in order to get some result we have to truncate the infinite dimensional matrix at some given N, so that $|m, n| \leq N$.
But recalling the discussion made in section 3.1 we know that the resonance occurring, for example, at ω_1 is *only* given by the intersection of the modes $m = \pm 1$. So the idea is to truncate the above matrix in the most brutal way: take $N = 1$. Clearly the result of such analysis will give us information only about the behaviour of the first resonant frequency at increasing h/d ratio, but actually that's all we're interested in.
So our analysis restrict to the coefficients labelled by $m = \pm 1$. The momentum required to couple the two modes, i.e. $\pm 2q$ will be provided by harmonics of the surface modulation through the c_n, d_n coefficients involved in the computation. It is nice to observe that the resulting coupling problem between modes with the same energy looks very similar to the usual quantum mechanics perturbation approach to the computation of energy levels splitting.
First of all, the coefficients of functions $c(x)$ and $d(x)$ are calculated as follows:
assume that the grating profile is given by

$$s(x) = \frac{h}{2}\sin(qx), \qquad h = \text{ grooves depth}, \qquad q = \frac{2\pi}{d}$$

then, since $s'(x) = hq/2\, cos(qx)$, the small parameter that justifies this method to be a "perturbation" method is

$$a = \frac{hq}{2}$$

With this definition the functions $c(x)$ and $d(x)$ become:

$$c(x) = \frac{1}{1+s'^2} = \frac{1}{1+a^2\cos^2(qx)} \simeq \frac{1}{1+\frac{a^2}{2}} - \frac{a^2}{4}\cos(2qx) = \eta - \frac{a^2}{4}\left(e^{2iqx} + e^{-2iqx}\right)$$

$$d(x) = \frac{s'}{1+s'^2} = \frac{a\cos(qx)}{1+a^2\cos^2(qx)} \simeq \frac{a}{2}\left(e^{iqx} + e^{-iqx}\right) - \frac{a^3}{8}\left(e^{3iqx} + e^{-3iqx}\right)$$

Thus the coefficients we need are:

$$\begin{cases} c_0 = \eta & c_{\pm 1} = 0 \\ c_{\pm 2} = \dfrac{a^2}{4} & c_{\pm 3} = 0 \end{cases} \qquad \text{and} \qquad \begin{cases} d_0 = 0 & d_{\pm 1} = \dfrac{a}{2} \\ d_{\pm 2} = 0 & d_{\pm 3} = -\dfrac{a^3}{8} \end{cases} \tag{3.23}$$

The matrix of coefficients is given by

$$\mathbb{T} = \left(\begin{array}{cc|cc} \alpha_1 d_0 & \alpha_{-1} d_2 & c_0 & c_2 \\ \alpha_1 d_{-2} & \alpha_{-1} d_0 & c_-2 & c_0 \\ \hline -\alpha_1^2 c_0 + \varepsilon k^2 & -\alpha_1 \alpha_{-1} c_2 & \alpha_1 d_0 & \alpha_1 d_2 \\ -\alpha_{-1}\alpha_1 c_{-2} & -\alpha_{-1}^2 c_0 + \varepsilon k^2 & \alpha_{-1} d_{-2} & \alpha_{-1} d_0 \end{array}\right) \tag{3.24}$$

that yields to:

$$\mathbb{T} = \begin{pmatrix} 0 & 0 & \eta & \frac{a^2}{4} \\ 0 & 0 & \frac{a^2}{4} & \eta \\ -q^2\eta + \varepsilon k^2 & q^2\frac{a^2}{4} & 0 & 0 \\ q^2\frac{a^2}{4} & -q^2\eta + \varepsilon k^2 & 0 & 0 \end{pmatrix} \tag{3.25}$$

The characteristic polynomial of the above matrix is

$$P(\lambda) = \left[\left(a^2 + 4\eta\right)\left(4k^2\epsilon + q^2\left(a^2 - 4\eta\right)\right) - 16\lambda^2\right]\left[\left(a^2 - 4\eta\right)\left(q^2\left(a^2 + 4\eta\right) - 4k^2\epsilon\right) - 16\lambda^2\right] \tag{3.26}$$

whose solutions are:

$$\begin{cases} \lambda_+^2 = & -\left(\eta + \dfrac{a^2}{4}\right)\left(\eta q^2 - \varepsilon k^2 - \dfrac{a^2 q^2}{4}\right) \\ \lambda_-^2 = & -\left(\eta - \dfrac{a^2}{4}\right)\left(\eta q^2 - \varepsilon k^2 + \dfrac{a^2 q^2}{4}\right) \end{cases} \tag{3.27}$$

Thus, defining $\zeta_\pm = \eta \pm \frac{a^2}{4}$ the associated eigenvectors read:

$$\phi_1 = \begin{pmatrix} -\zeta_+ \\ -\zeta_+ \\ \lambda_+/\zeta_+ \\ \lambda_+/\zeta_+ \end{pmatrix},\ \phi_2 = \begin{pmatrix} \zeta_+ \\ \zeta_+ \\ \lambda_+/\zeta_+ \\ \lambda_+/\zeta_+ \end{pmatrix},\ \phi_3 = \begin{pmatrix} \zeta_- \\ -\zeta_- \\ -\lambda_-/\zeta_- \\ \lambda_-/\zeta_- \end{pmatrix},\ \phi_4 = \begin{pmatrix} -\zeta_- \\ \zeta_- \\ -\lambda_-/\zeta_- \\ \lambda_-/\zeta_- \end{pmatrix} \tag{3.28}$$

Now that we have the eigenvectors of matrix $\mathbb{T}$ we can express the solution as

$$\xi(u) = A\phi_1 e^{i\lambda_+ u} + B\phi_2 e^{-i\lambda_+ u} + C\phi_3 e^{i\lambda_- u} + D\phi_4 e^{-i\lambda_- u}$$

From equation 3.27 we notice that in the material, i.e. for $u < 0$, the dielectric function is negative, thus both λ_+ and λ_- are negative. So, in order to have finite amplitude solutions in $u < 0$, we have to set $A = C = 0$. Furthermore, since the differential problem is linear (see section 2.2) the solution has to satisfy boundary conditions:

$$\zeta(u = 0^+) = \zeta(u = 0^-) \qquad \Longrightarrow \qquad \begin{pmatrix} F(u = 0^+) \\ G(u = 0^+)/\varepsilon_a \end{pmatrix} = \begin{pmatrix} F(u = 0^-) \\ G(u = 0^-)/\varepsilon_p \end{pmatrix} \tag{3.29}$$

Thus, it's straightforward that the first two components of each eigenvalues give no further information on the field coefficients, while the last two provide:

$$\begin{cases} \frac{1}{\varepsilon_a}\left[B\frac{\lambda_{1+}}{\zeta_+} - D\frac{\lambda_{1-}}{\zeta_-}\right] = \frac{1}{\varepsilon_p}\left[B\frac{\lambda_{2+}}{\zeta_+} - D\frac{\lambda_{2-}}{\zeta_-}\right] \\ \frac{1}{\varepsilon_a}\left[B\frac{\lambda_{1+}}{\zeta_+} + D\frac{\lambda_{1-}}{\zeta_-}\right] = \frac{1}{\varepsilon_p}\left[B\frac{\lambda_{2+}}{\zeta_+} + D\frac{\lambda_{2-}}{\zeta_-}\right] \end{cases} \tag{3.30}$$

Sum and subtraction of the above equations lead to

$$\begin{cases} \frac{\lambda_{1+}}{\varepsilon_a} = \frac{\lambda_{2+}}{\varepsilon_p} \\ \frac{\lambda_{1-}}{\varepsilon_a} = \frac{\lambda_{2-}}{\varepsilon_p} \end{cases} \tag{3.31}$$

which is an extension of the flat reflection case

$$\frac{\lambda_1}{\varepsilon_a} = \frac{\lambda_2}{\varepsilon_p}$$

It is clear then that the two eigenvalues λ_+^2, λ_-^2 correspond to the no-more-degenerate frequencies ω_+, ω_-. Substitution of the last into eq. 3.31 yields:

$$\begin{cases} \frac{1}{\varepsilon_a^2}\left(\eta q^2 - \varepsilon_a\left(\frac{\omega_+}{c}\right)^2 - \frac{a^2q^2}{4}\right) = \frac{1}{\varepsilon_p^2}\left(\eta q^2 - \varepsilon_p\left(\frac{\omega_+}{c}\right)^2 - \frac{a^2q^2}{4}\right) \\ \frac{1}{\varepsilon_a^2}\left(\eta q^2 - \varepsilon_a\left(\frac{\omega_-}{c}\right)^2 + \frac{a^2q^2}{4}\right) = \frac{1}{\varepsilon_p^2}\left(\eta q^2 - \varepsilon_p\left(\frac{\omega_-}{c}\right)^2 + \frac{a^2q^2}{4}\right) \end{cases} \tag{3.32}$$

Again, sum and subtraction provide

$$\begin{cases} \frac{1}{\varepsilon_a^2}\left(2\eta q^2 - \varepsilon_a\left[\left(\frac{\omega_+}{c}\right)^2 + \left(\frac{\omega_-}{c}\right)^2\right]\right) = \frac{1}{\varepsilon_p^2}\left(2\eta q^2 - \varepsilon_p\left[\left(\frac{\omega_+}{c}\right)^2 + \left(\frac{\omega_-}{c}\right)^2\right]\right) \\ \frac{1}{\varepsilon_a^2}\left(\left[\left(\frac{\omega_+}{c}\right)^2 + \left(\frac{\omega_-}{c}\right)^2\right] + \frac{a^2q^2}{2}\right) = \frac{1}{\varepsilon_p^2}\left(\left[\left(\frac{\omega_+}{c}\right)^2 + \left(\frac{\omega_-}{c}\right)^2\right] + \frac{a^2q^2}{2}\right) \end{cases} \tag{3.33}$$

Then, defining

$$\frac{\overline{\omega^2}}{c^2} = \frac{1}{2}\left[\left(\frac{\omega_+}{c}\right)^2 + \left(\frac{\omega_-}{c}\right)^2\right] \qquad \frac{\Delta\omega^2}{c^2} = \frac{1}{2}\left[\left(\frac{\omega_+}{c}\right)^2 - \left(\frac{\omega_-}{c}\right)^2\right]$$

we get

$$\begin{cases} \left(\frac{1}{\varepsilon_p} - \frac{1}{\varepsilon_a}\right)\frac{\overline{\omega^2}}{c^2} = \left(\frac{1}{\varepsilon_p^2} - \frac{1}{\varepsilon_a^2}\right)\eta q^2 \\ \left(\frac{1}{\varepsilon_p} - \frac{1}{\varepsilon_a}\right)\frac{\Delta\omega^2}{c^2} = \left(\frac{1}{\varepsilon_p^2} - \frac{1}{\varepsilon_a^2}\right)\frac{a^2q^2}{4} \end{cases} \tag{3.34}$$

and, after simplifying

$$\begin{cases} \dfrac{\overline{\omega^2}}{c^2} = \left(\dfrac{1}{\varepsilon_p} + \dfrac{1}{\varepsilon_a}\right)\eta q^2 \\ \dfrac{\Delta\omega^2}{c^2} = \left(\dfrac{1}{\varepsilon_p} + \dfrac{1}{\varepsilon_a}\right)\dfrac{a^2 q^2}{4} \end{cases} \tag{3.35}$$

Now, after recalling that the plasmon dispersion relation at normal incidence for the unperturbed case was

$$n^2 q^2 = \frac{\omega_n^2}{c^2}\frac{\varepsilon_a \varepsilon_p}{\varepsilon_a + \varepsilon_p} \qquad \Longrightarrow \qquad \frac{\omega_1^2}{c^2} = \left(\frac{1}{\varepsilon_p} + \frac{1}{\varepsilon_a}\right) q^2 \tag{3.36}$$

the new central frequency and energy gap become respectively:

$$\begin{cases} \dfrac{\overline{\omega^2}}{c^2} = \left(\dfrac{\omega_1}{c}\right)^2 \dfrac{1}{1 + a^2/2} & \text{Central frequency position} \\ \dfrac{\Delta\omega^2}{c^2} = \left(\dfrac{\omega_1}{c}\right)^2 \dfrac{a^2}{4} & \text{Energy gap}[1] \end{cases} \tag{3.37}$$

Thus, at the end of the day we are able to predict a "red shift" of the resonant frequencies, given by the fact that $\eta < 1$.

This red shift can be qualitatively seen as a consequence of the total grating surface length being greater than the flat mirror: since the "unit distance" the plasmon wave has to travel in a given time interval is greater than in the flat case, the phase velocity of the wave will be correspondently smaller. Thus, if we recall that the plasmon momentum is fixed by the matching condition and $v_\phi = \omega/k$, we understand why it's right to expect that the resonant frequency will decrease as soon as the grating h/d ratio increases.

The amount of this frequency shift is given by the following formula:

$$\boxed{\overline{\omega} = \omega_1 \left[1 - \left(\frac{hq}{4}\right)^2\right]} \tag{3.38}$$

which is in fair agreement (see fig. 3.7) with our numeric result up to a factor 3:

[1] the computed energy gap is one order of magnitude smaller than the one predicted in [W. L. Barnes 1996]. Since it is not visible at all in our simulations, we will omit to take it into consideration

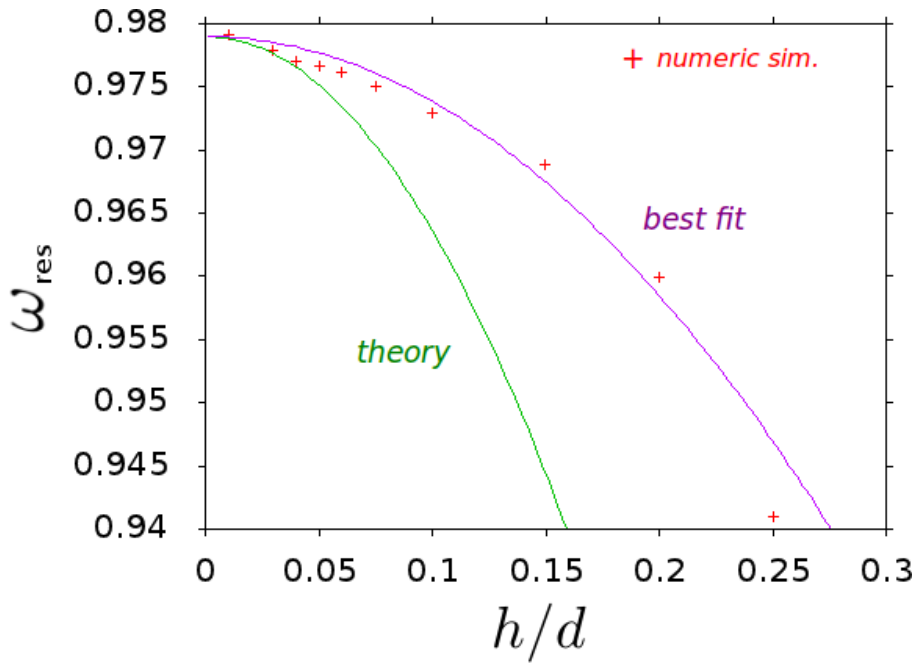

Figure 3.7: Red-shift of resonant frequency at increasing h/d

The reasons for this mismatch is that in our calculation we have only considered the modes $m = \pm 1$ as the only terms providing second order correction in h/d. This is not completely correct, since taking into consideration the interaction between modes $m = 1, 2$ and $m = -1, -2$, the matrix element $d_{\pm 1} \propto hq$ in equations 3.23 enters the calculation, thus in the end we obtain an additional second order h/d term that could adjust the factor in parentheses. The investigation of the much more cumbersome "four-modes" interaction wasn't reported here for lack of time, but will object of further study.

Chapter 4

Particle dynamics

In this section we apply the concept of surface plasmon resonances to the field of high power laser-matter interaction. First of all we show how the surface plasmon resonance excitation can be relevant in the framework of laser matter interaction (see Appendix C). Then we describe the numerical method we use to study the particle acceleration problem and we'll eventually show the results obtained.

4.1 High power laser matter interaction by numbers

Modern high power lasers generally make use of the so-called "chirped pulse amplification" technique, invented by [Mourou 1985] and co-workers, which permits an amplification of the laser pulse to very high optical intensities while avoiding excessive non linear pulse distortions or optical damage. We can illustrate the main features of the physics involved in the interaction of such lasers with matter (we are interested in solid targets) by very simple considerations.
A chirped amplified laser usually reaches high power peaks because they release the provided amount of energy in a very short time. For example the ELFIE laser of LULI (Laboratoire pour l'utilisation des lasers intenses) delivers an energy amount $\Delta E = 30J$ in a time lapse $\Delta t = 300fs$. This allows to reach peak powers of the order of $10^{14}W$. Both these two numbers

$$P = 10^{14}W \qquad \Delta t = 0.3ps$$

are enough to fix the physical framework of the problem:

- ▷ **Short Time** The rapidly ionized material in front of the target starts to expand into the vacuum side at the typical speed of the rarefaction phenomena, which for a plasma is given by the ion-sound velocity. Thus after a time interval of the order of the typical pulse duration, the plasma has managed to expand over a distance

$$c_s \Delta t = \sqrt{\frac{k_b T_e}{m_i}} \Delta t \sim 10^7 \frac{\mathrm{cm}}{s} \times 10^{-12} s \sim 0.1 \mu m \qquad \text{for } T_e = 1keV$$

that's smaller than the usual wavelengths $\lambda \sim 1\mu m$. Thus the first assumption we can make is that of a *step-like density profile* plasma. The second one is that if the plasma has no time to expand, its density will be of the order of the solid density, i.e.

$$n_e \sim 10^{23} \mathrm{cm}^{-3}$$

But if we compare this with the critical (or cut-off) density

$$n_{cr}(\lambda \sim 1\mu m) \sim 10^{21} \mathrm{cm}^{-3}$$

we realize that

$$\epsilon(\omega) \simeq 1 - \frac{\omega_p^2}{\omega^2} = 1 - \frac{n_e}{n_{cr}(\lambda)} < 0 \tag{4.1}$$

so that no light can propagate into the plasma. In this condition the plasma is said to be *overdense*.

▷ **High Power** When the high power laser beam is focalised into a spot of the order of $10\lambda \sim 10\mu m$, the laser intensity can reach (and overcome)

$$I_L \sim 10^{18} \frac{W}{\mathrm{cm}^2}$$

But recalling that

$$I = \frac{c}{4\pi}|\mathbf{E}|^2 = \frac{c}{4\pi}\frac{\omega^2}{c^2}|\mathbf{A}|^2 = \frac{c|\mathbf{A}|^2}{\pi\lambda^2}$$

the dimensionless parameter a_0 take the form:

$$a_0 = \frac{eA_0}{mc^2} = 0.85 \times \left(\frac{I\lambda^2}{10^{18}\, W\ \mathrm{cm}^2}\right)^{1/2} \simeq (I_{18}\lambda_{\mu m}^2)^{1/2} \underset{\text{for } I\sim 10^{18}}{\sim} 1 \tag{4.2}$$

Thus, the number 10^{18} can be seen as the threshold for the laser intensity to drive a *relativistic* dynamics of the charges involved. This is because the relativistic factor for the free charge acceleration (see eq. C.24 and discussion in Appendix C)

$$\gamma = 1 + \frac{a_0^2}{2}$$

starts to become greater than one.

In summary, just knowing the power released and the pulse duration of the laser we are led to conclude that the interaction process with the laser target has to be described as a *relativistic interaction with an overdense step-like plasma.*

As already explained in the Introduction, the most efficient mechanism to couple the laser energy to an overdense plasmas is through the injection of energetic particles into the target, that heat the plasma while loosing the acquired energy. We won't deal with the problem of energy and momentum transport in an ionized material crossed by relativistic particles. Here we will concentrate on how to improve this acceleration, whose key feature is to occur near the target surface. For this reason it seems natural to introduce a modulation to the target surface, since we have seen that when surface plasmon resonance are excited, a great part of the electromagnetic energy can be confined in the proximity of the surface. The bigger the surface fields, the higher the acceleration. The higher the acceleration, the better the energy transfer!

The question arising now is: how can the target's periodic structure survive while being ablated under the laser radiance? As we showed before, the ionized material in front of the target has no time to expand, thus we can assume that the periodicity of the structure will be conserved during the interaction. On the other hand it is clear that the modulation depth cannot be as small as in usual gratings, where the depth over pitch ratio is $h/d \sim 1/100$, otherwise the coupling effects discussed in the previous chapters will not be relevant since the laser radiance will wipe out the periodic modulation. This is the reason for why throughout our work we have taken the parameter h/d in the range $0.05 \div 0.2$.

4.2 The particle acceleration concept in external potential

The principle of particle acceleration by a wave, either electromagnetic or electrostatic (or both) is illustrated in fig. 4.1, where a point particle "feels" the presence of an external potential. The similarity with surfing helps to visualize the acceleration mechanism.

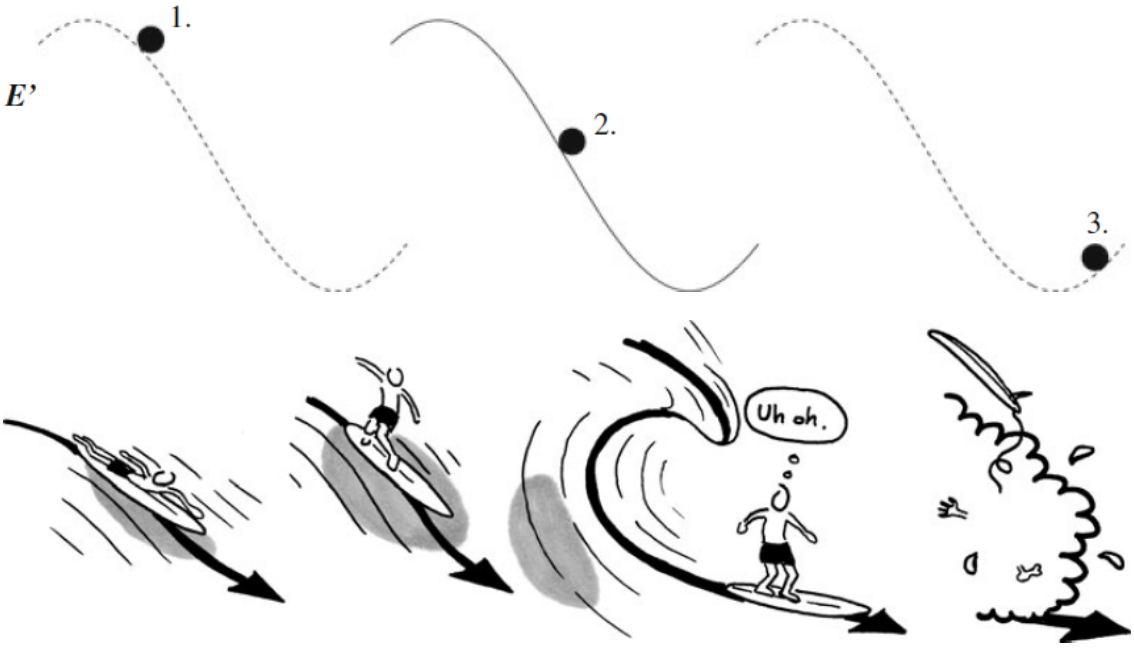

Figure 4.1: Energy gain of a particle in a wave potential

How does the surfer in picture gain velocity from the sea wave? It is necessary for the surfer to have some initial velocity along the propagation direction of the wave. If possible, the initial velocity should be equal to the phase velocity of the wave, because in its rest frame the surfer would see a constant field which can provide a net acceleration, in contrast to an oscillating field for which the acceleration averages to zero over a cycle. Of course, the process of acceleration has a negative feedback because a change in the surfer's velocity leads to dephasing from the wave: something a surfer knows to be not always enjoyable. On the other hand, if the surfer were "relativistic", i.e. its velocity were close to c, the dephasing would be much less pronounced, since it would be energetically difficult to gain further speed. Thus, a relativistic surfer would ride the wave for a much longer distance than a "human" surfer. Back to physics, the high power element turns in our favour when dealing with particles acceleration.
The above example suggests us two necessary conditions for an electromagnetic wave to efficiently accelerate a charged particle: there must be an electric field component along the propagation direction, and the phase velocity must be such that an optimal phasing between the wave and the particle can occur. These conditions can be met in a surface wave and were the reason why in the 70's they were so appealing to accelerator physicists. However, we already discussed the interest shift from particle acceleration

along the material surface to injection of the accelerated particles *into* the material. Here, the quantity of relevance is provided by the quiver energy W discussed in Appendix C, since several experimental observations suggest that the typical order of magnitude of the fast electron energy is of the order of the cycle-averaged oscillation energy in the electric field of the laser in vacuum. Indeed, it plays the role of the external potential felt by the particle which is going to be accelerated and will be the quantity of reference in the next section, when we will use it to evaluate and compare with the numerical result obtain with our code.

4.3 Numerical solution of acceleration problem by test particles approach

The test particle approach consists in studying the motion of a charged particle under the influence of the e.m. fields produced by the reflection on a modulated target, assuming them as *external fields*. Clearly this represents a rough simplification of the self-consistent problem, in which the field induced by the laser is depleted by the particles acceleration. Thus, the limit of this approach is that it cannot be able to predict the actual coefficient of absorption efficiency, since we are not able to estimate how many particles will be accelerated in the real process.
Indeed, if the absorption coefficient can be simply expressed as

$$\eta = \frac{E_{abs}}{E_L}$$

and the absorbed energy is

$$E_{abs} = \int \varepsilon(p)\mathrm{f}(\mathbf{p})\, \frac{d\mathbf{p}}{m_e} \tag{4.3}$$

we don't know the distribution function $\mathrm{f}(\mathbf{p})$, since we don't know how many particles have to be distributed. This comes from the fact that the FDTD code we have developed solves a macroscopic set of equations (Maxwell's equations in *continuous* media), thus we have to choose the number of particles to initialize in the external field at our discretion (obviously this means that we put as many particles as our computer is able to track in a reasonable computation time).

What can we learn from a test particle simulation? We can obtain the average energy the test particle can gain from the vacuum acceleration, and investigate whether there is a connection between the acceleration process and the phase of the fields the particles are initialized into.
To achieve this we performed our simulations initializing a number $N \cdot T$ of test particles in the following way:

- ▷ Grating sampling:

  We initialize a number N of particles along one period of the grating surface, with thermal velocities (picked at random from a Gaussian distribution) along the surface

normal. In this way, the coordinates and velocities of the initialized particles are:

$$(x_i, y_i) = \left(\frac{h}{2}\cos\left[i\frac{d}{N}\right], i\frac{d}{N}\right) \qquad (v_{x,i},\, v_{y,i}) = (v_{th}, 0) \quad \text{where } v_{th} = \sqrt{\frac{k_B T_e}{m_e}} \tag{4.4}$$

▷ Phase sampling:

We re-initialise the bunch of N particles in the way described above each after a time interval

$$\Delta T = \frac{t_{end} - t_0}{T}$$

where T is the total number of re-initialization. Clearly ΔT has to be greater than the temporal resolution of the FDTD code.

With this set up, we solve the equation of motion

$$\frac{d\mathbf{p}_{i,m}}{dt} = q\left[\mathbf{E}(\mathbf{x}_i, t, \phi_m) + \frac{\mathbf{u_{i,m}}}{c} \times \mathbf{B}(\mathbf{x}_i, t, \phi_m)\right] \quad \text{where } \phi_m = m\frac{t_{end} - t_0}{T} \tag{4.5}$$

The above equation indicates that the i^{th} bunch of N electrons feels the same fields as the $(i-1)^{th}$ bunch, but with a phase delay $\phi = \Delta T$. This is equivalent to running the code just once, but initializing the electrons according to the following scheme:

→ First electrons bunch runs for $t_{end} - t_0$ starting at $t = t_0$

→ 2^{nd} electrons bunch runs for $t_{end} - (t_0 + \Delta T)$ starting at $t = t_0 + \Delta T$

⋮

→ m^{th} electrons bunch runs for $t_{end} - (t_0 + m\Delta T)$ starting at $t = t_0 + m\Delta T$

⋮

→ $(T-1)^{th}$ electrons bunch runs for ΔT starting at $t = t_{end} - \Delta T$

→ T^{th} electrons bunch doesn't move at all

When the simulation ends, we divide the particles having given momentum and positions and plot the number density into a phase space coordinate plot, in order to get an idea of how the distribution function looks like.

4.4 Results

4.4.1 Normal incidence

In figure 4.2 is shown a simulation of particle acceleration driven by a laser pulse of amplitude $a_0 = 1$ which impinges on a 25 times overdense plasma, with electron temperature

$T_e = 1keV$ (ion are kept still, as a neutralizing background). These values have been chosen to compare our simulation with the usual parameter used in PIC codes. The optical response is described by the dielectric constant:

$$\epsilon(\omega) = 1 - \frac{\omega_p^2}{\omega(\omega - i\nu_{ei})} \tag{4.6}$$

with the values:

- ▷ *Plasma frequency:* $\omega_p = 5.6 \times 10^4 n_e^{1/2}[\mathrm{cm}^{-3}]s^{-1} \simeq 8 \times 10^{15} s^{-1}$
- ▷ *Normalization frequency:* $\omega_0 = 2\pi \times 10^{14} s^{-1}$
- ▷ *Collisional frequency:* $\nu_{ei} = 10^{-7} Z^2 n_i[\mathrm{cm}^{-3}] T_e^{-3/2}[eV] s^{-1} \simeq 7 \times 10^{13} s^{-1}$

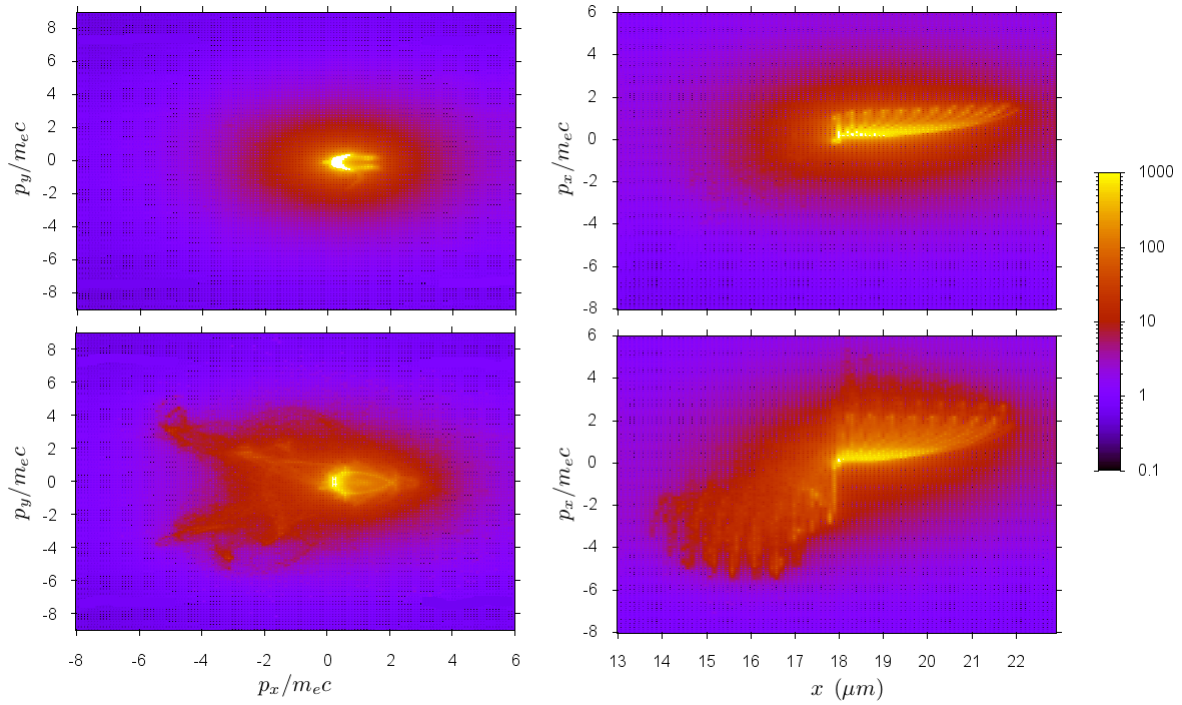

Figure 4.2: Test particle simulation of $h(p_x, p_y)$ and $g(x, p_x)$ for not-resonant (upper row) and resonant frequency (lower row)

In first and second columns are respectively shown the contour plot of $g(x, p_x)$ and $h(p_x, p_y)$, defined as follows:

$$h(p_x, p_y, t) = \int \mathrm{f}(\mathbf{x}, \mathbf{p}, t)\, d\mathbf{x} \qquad \text{and } g(x, p_x, t) = \int \mathrm{f}(\mathbf{x}, \mathbf{p}, t)\, \frac{dp_y}{m_e}\, dy \tag{4.7}$$

evaluated after $t = 5\mathcal{T}$ laser periods.
On the other hand, the upper row of figures change from the lower only for the value of the normalized frequency ω/ω_0. In the first raw, the normalized laser frequency is $\omega/\omega_0 = 1.1$,

while in the second $\omega/\omega_0 = 0.978$, which, according to figure 3.6, are respectively a not-resonant and a resonant frequency for the surface plasmon excitation. The difference in the maximum energy achieved by the particles is clearly different between the two different cases. In particular, we notice a highly enhanced presence of particles in the vacuum region, which reflects the fact that the surface plasmon has a greater extension into the vacuum side than an ordinary evanescent field produced by the grating curvature.
This acceleration enhancement is not dependant on the amplitude over pitch parameter h/d of the grating. This is clearly shown in figures 4.3a - 4.3b, where we plot the numerically computed function:

$$n(\epsilon) = \frac{dN}{d\epsilon}, \text{where } N = \int n\, d\epsilon = \#\text{ test e}^-,\ \epsilon = \frac{E_c}{m_e c^2} = \sqrt{1+|p|^2} - 1 \tag{4.8}$$

for different h/d ratios, for both the resonant and not-resonant case:

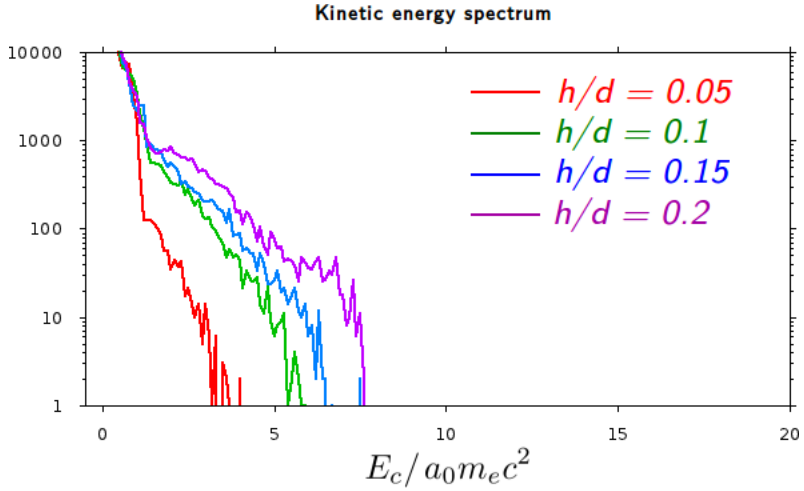

(a) *Kinetic energy of accelerated electrons when no plasmon resonance occurs*

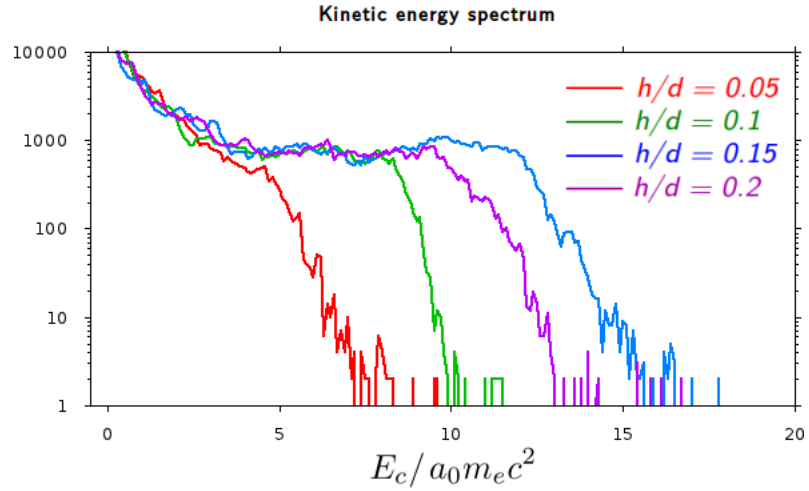

(b) *Kinetic energy of electrons accelerated in the plasmonic field*

Figure 4.3: Logarithmic electrons' energy distribution for different values of h/d ratio. The average energy increase is clearly visible and doesn't depend on the grating depth

It is remarkable that particle acceleration enhancement occurs when the plasmon surface resonance is excited, *regardless of the grating amplitude*.

4.4.2 Oblique incidence

For oblique incidence we obtain results which agree with those of the previous section. Before presenting them we'd like to point out that from fig. 3.6 we notice that even for small angles of incidence the degeneracy of the modes $m = \pm 1$ is removed (by symmetry breaking). Thus if we shine the grating with a broadband wave-packet (as in the simulation for normal incidence) incident at a small angle θ, we will be able to observe a splitting of the resonant frequencies. This is clearly shown in figure 4.4:

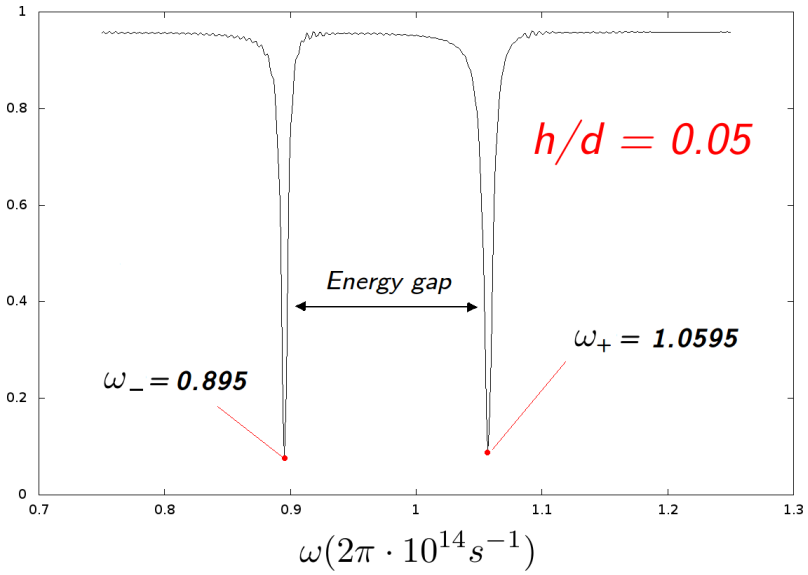

Figure 4.4: Gap opening at first resonant frequency for $\theta = 5°$

The difference with the previous case is that here is impossible to excite both the modes with a single monochromatic pulse. Then, since there will no longer be two counter-streaming identical modes (generating a *standing* surface wave), the surface mode will propagate with phase velocity given by

$$v_\phi = \frac{\omega}{k_{sp}} = c\,\frac{k}{k\sin\theta + nq} \tag{4.9}$$

Formula 4.9 is valid for both resonant and evanescent modes. This leads to the following surprising results: first of all, a small deviation of the incidence angle from the orthonormal case produces an abrupt change in the phase velocity of the surface wave. For example a change from $\theta = 0 \to 5°$ and $\omega/qc = 0.979 \to 0.895$ produces a phase velocity change from $0 \to -0.97\,c$! The other surprising thing is the minus sign the phase velocity can acquire: this means that the SPR wave-vector can be opposite to the parallel component of the incident light wave-vector, thus violating the momentum conservation! The trick is that, as already pointed out, the conserved quantity is not $k_\parallel$ (the momentum), but $k_\parallel \pm |n|q$

(the quasi-momentum), thus the surface modulation can provide the necessary "negative momentum" for the surface wave to be counter-streaming to the parallel component of the incident wave.
Another peculiarity of the oblique incidence is that the dispersion relation cannot be expressed in the form $\omega = f(k_{sp})$, i.e. is not analytically solvable:

$$k_{sp}^2 = \frac{\omega^2}{c^2}\frac{\omega^2 - \omega_p^2}{2\omega^2 - \omega_p^2} \quad \Longrightarrow \quad \left(\frac{\omega}{c}\sin\theta + nq\right)^2 = \frac{\omega^2}{c^2}\frac{\omega^2 - \omega_p^2}{2\omega^2 - \omega_p^2} \quad \text{implicit function of } \omega \tag{4.10}$$

Graphic solution of eq. 4.10 for $\theta = 5°$ yields:

$$\omega_- = 0.905 \qquad \omega_+ = 1.067$$

which agrees up to 1% with the results of the numeric simulation.
When we put electrons in the surface fields with the numerical scheme described before, we observe that the acceleration is again much more enhanced when the SPR is excited, regardless of the h/d parameter:

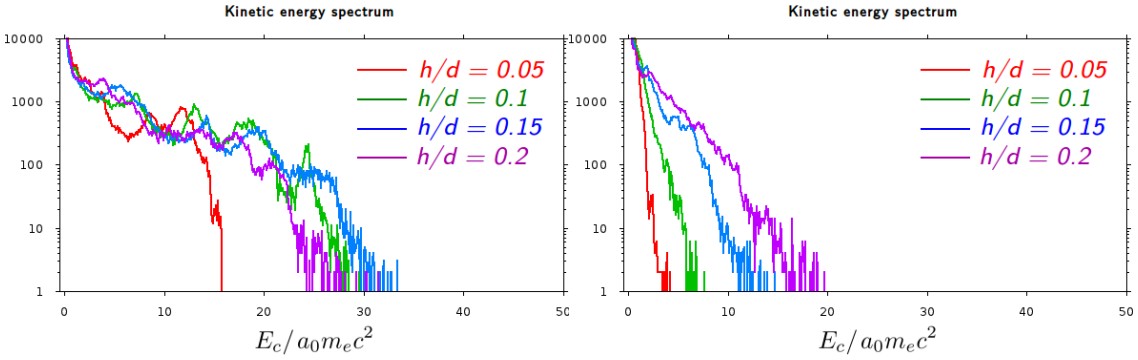

(a) *Low energy resonance* $\omega = \omega_-$

(b) *Incident frequency* $\omega = (\omega_- + \omega_+)/2$

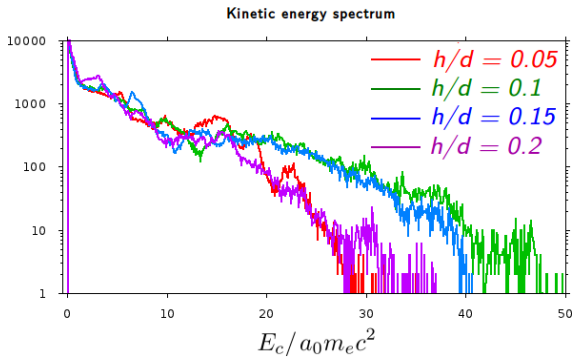

(c) *High energy resonance* $\omega = \omega_+$

Figure 4.5: Kinetic energy distribution of accelerated electrons for different frequencies

The pictures showing the electrons acceleration in the resonant fields presents the same plateau characteristic of the normal incident case. One may think that those results are not surprising, since the angle of incidence is not too far from zero, but what is peculiar here

are the much higher energies that the electrons acquire in the resonant fields if confronted with the normal incidence case. This is because at oblique incidence, even for very small angles, we are able to excite only one of the two $\omega_{\pm}$, thus we accelerate particle in a *propagating* surface wave, instead of in a standing one. As shown in the introduction of this chapter, this corresponds to having in the reference frame moving with the phase speed ω/k_{sp} a potential Φ', whose maximum value provides us the quantity W':

$$W' = \max(\Phi') \quad \xrightarrow{\text{Lab frame}} \quad W = \gamma W' \quad \text{where } \gamma = \frac{\omega_p^2}{\omega^2} - 1 \gg 1 \tag{4.11}$$

which tells us that the maximum energy an electron can acquire in the oblique incidence case is a *gamma* factor higher than in the normal case. Thus, in the oblique case, a higher energy is gained because the electrons actually "surf" a propagative surface wave with move at speed very close to c. This is confirmed also by simulation at incident angle far from zero. In picture 4.6 is shown a simulation with the same parameters as before except for the angle of incidence $\theta = 30°$, for which the resonant frequency is $\omega_{res}/\omega_0 = 0.6626$.

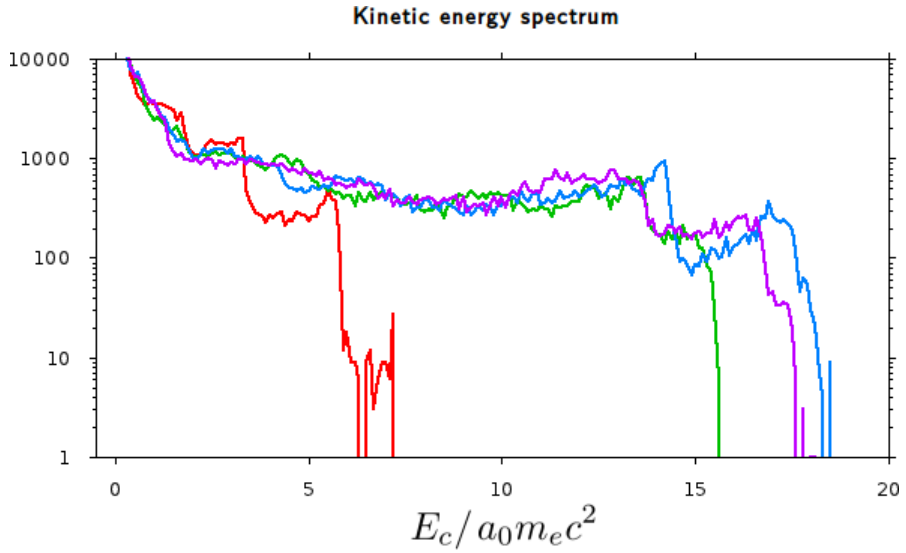

Figure 4.6: Electrons energy distribution for $\theta = 30°$. Legend is the same as in the previous figures

However, we have to remark that higher mean energies in the oblique incidence case doesn't correspond necessarily to absorption coefficients that are greater than the normal incidence case. That's because it is not obvious that the injection of accelerated electrons in the oblique case is the same as in the normal one. On the contrary we should expect that in the oblique case the number of electrons accelerated *along* the modulated surface is greater than in the normal case, since in the former case the surface wave is propagating along the surface, while in the latter the wave is a standing one. This is clearly observable in figure 4.7:

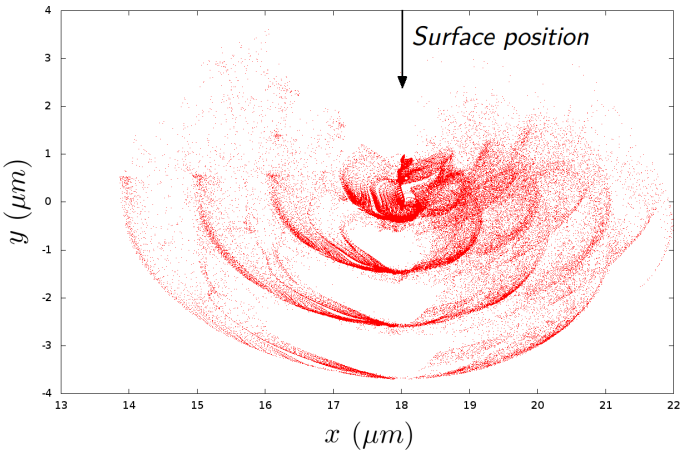

(a) *Low energy resonance* $\omega = 0.895$*: down-streaming*

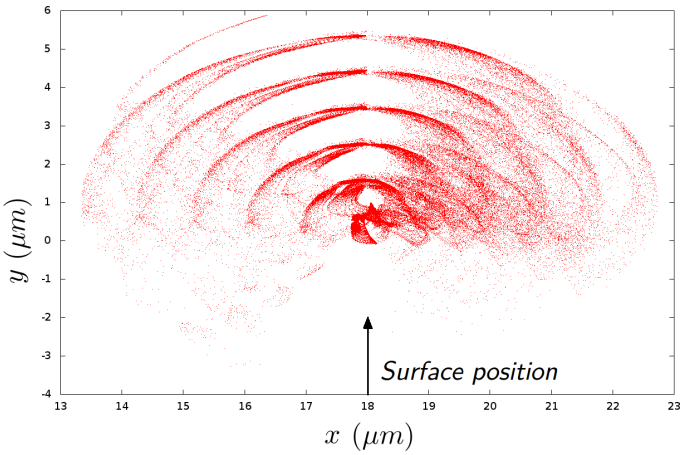

(b) *High energy resonance* $\omega = 1.059$*: up-streaming*

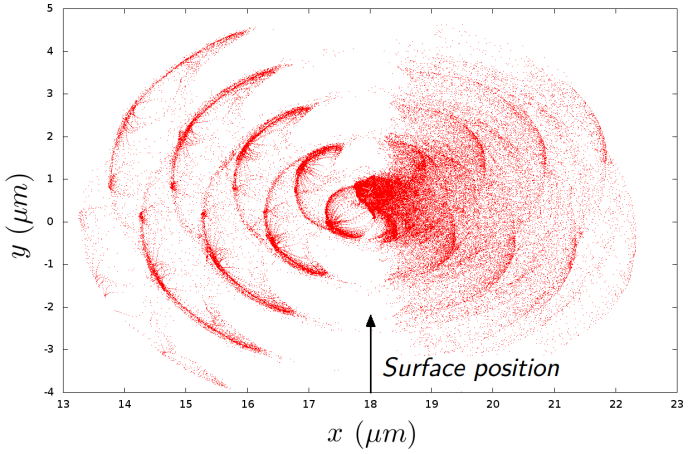

(c) *Normal incidence resonance* $\omega = 0.979$

Figure 4.7: Spatial distribution of accelerated electrons after 5 laser cycles. As described in section 4.3, the electrons are initialised along **one** period of the target modulation.

This is also an indirect numerical proof of the fact a surface wave can propagate upwards

or downwards according to its quasi-momentum.
We conclude this chapter by showing another interesting difference occurring between the normal incidence case and the oblique one, that is caused by the degeneracy breaking when the incidence occurs at an angle $\theta \neq 0$. We first report it in figure 4.8:

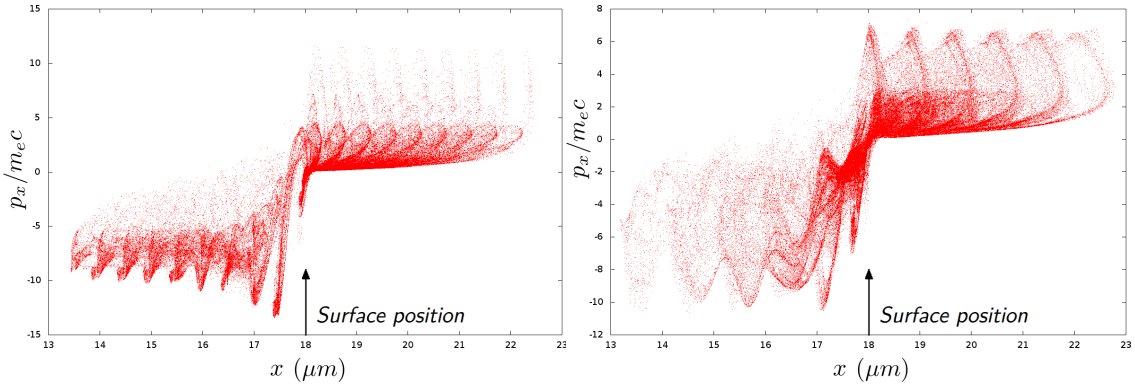

(a) *Normal incidence* (b) *Oblique incidence:* $\theta = 5°$

Figure 4.8: Comparison of functions $g(x, p_x)$ for the normal incident case and oblique one. The simulation runs for 5 periods of the respective resonant frequencies, which are $\omega/\omega_0 = 0.979$ and $\omega_+/\omega_0 = 1.049$

In the oblique incident case there are as many electrons "jets" injected into the plasma as the number of period the simulation runs ($t = 5T$ for both simulations), while in the normal incidence case the jets produced are *twice* as much as the laser period. This suggests a close resemblance with the 2ω injection mechanisms called "$\mathbf{J} \times \mathbf{B}$ heating", which is proper of normal incidence systems, and the ω "Brunel effect", which is effective at oblique incidence [Gibbon 1992].
However, this is not only a nice a similarity. From figure 4.7c it is evident that since at normal incidence the plasmon has no electric field along the surface, the acceleration is provided by the $\mathbf{v} \times \mathbf{B}$ term, which, with its 2ω electrons bunch production, is the single particle analogous of $\mathbf{J} \times \mathbf{B}$ heating. The same holds for oblique incidence, where there is only an electrons bunch per cycle produced(cfr. 4.7b - 4.7a).

Chapter 5

Conclusions

In this last chapter we briefly summarize the outline and results of this thesis work.

5.1 Summary

After having introduced (Chapter 2) the main techniques to describe the fields diffracted by a grating we have shown how the particular phenomenon of surface plasmon resonance (SPR) can occur, and why it appears only for p-polarised light (see fig. 5.1) and when a periodically modulated interface is present (Chapter 3).

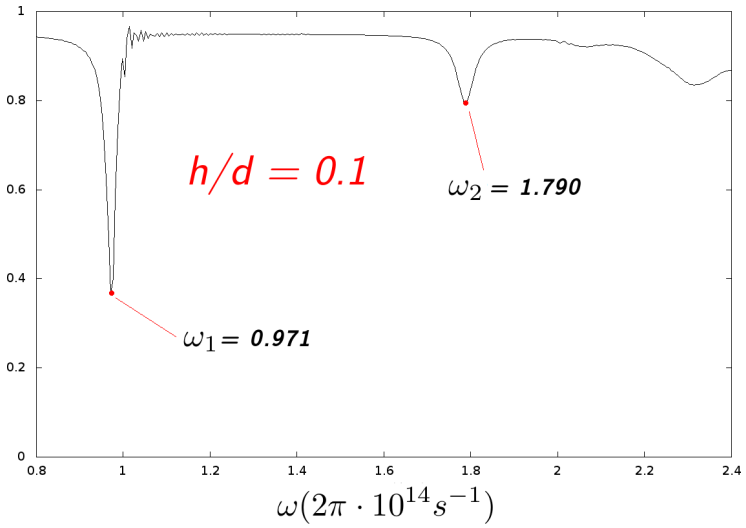

Figure 5.1: Simulation of the Reflectivity spectrum of p-polarised light normally incident on a diffraction grating with our FDTD code. While for most frequencies of the incident light the grating behaves like a mirror, for given frequencies the reflectivity coefficient drops to much lower values. Since no transmission occurs, the "missing" light is confined near the surface, revealing the presence of a surface plasmon resonance. The simulation parameters are: grating depth $h = 0.1\mu m$, grating pitch $d = 1\mu m$, normalized plasma frequency $\omega_p^2/\omega_0^2 = 25$, damping coefficient $\nu/\omega_0 = 0.1$, with $\omega_0 = 2\pi c/d$ the normalizing frequency

Then, we provided an original model to account for the dependence of the frequency shifts, observed in the numerical simulations of the reflectivity spectra, which occurs at increasing h/d ratio as a consequence of the interaction among different surface modes. This calculation was necessary since in high power laser-matter interaction the h/d parameter cannot be much smaller than unity.

▷ *Resonant frequencies formula at normal incidence*: solution of the intersection of plasmon dispersion curve and $k_{sp} = 0$ right. See fig. 5.2.

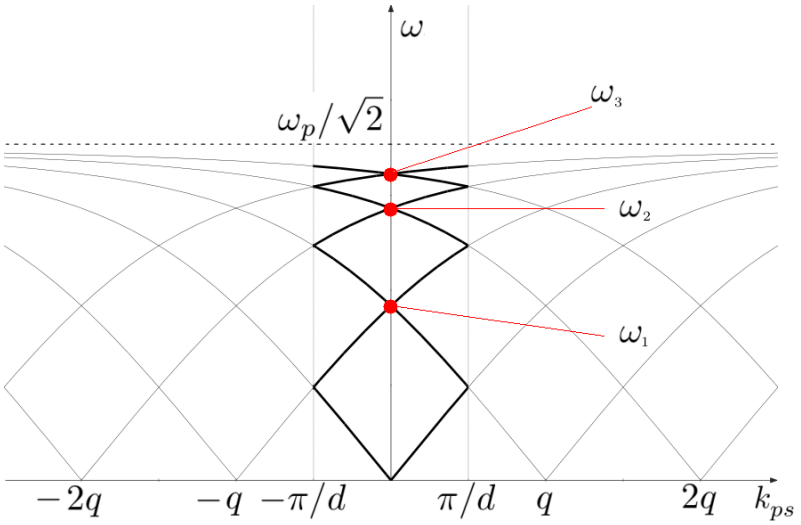

Figure 5.2: Graphic solution of plasmon-photon coupling at normal incidence

$$\omega_n^2 = \frac{\omega_p^2}{2} + n^2q^2c^2 - \sqrt{\frac{\omega_p^4}{4} + n^4q^4c^4} \tag{5.1}$$

▷ *Resonant frequencies shift*:

$$\overline{\omega} = \omega_1 \left[1 - \left(\frac{hq}{4}\right)^2\right] \tag{5.2}$$

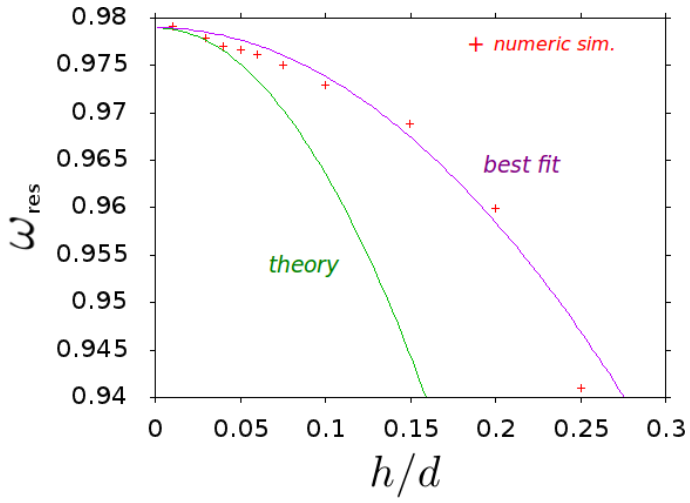

Figure 5.3: **Comment**: The analytical model could be improved by further (cumbersome!) calculation

Afterwards (in chapter 4) we have shown by means of simple dimensional analysis how the excitation of surface plasmon resonances can be relevant in the framework of high power laser matter interaction, in particular in the heating problem, in which the most efficient heating mechanisms are based on the injection of "vacuum accelerated" electrons.

Since in those mechanisms a crucial role is played by the fields near the plasma-vacuum interface, we have investigated the role of SPR excitation in the electrons acceleration enhancement observed with modulated targets by means of a two-step numerical technique: at first the surface fields produced by a modulated surface are studied with a FDTD electromagnetic code, considering the plasma a Drude metal (for details see Appendix A). After, the electrons motion in the surface fields is studied by a test particle approach.

With this numerical scheme we were able to show that the electrons dynamics is greatly sensitive to SPR excitation. In particular, the average kinetic energy acquired by the electrons in the resonant fields is much greater than in the not resonant case, and the energy distribution of the accelerated electrons shows an extended "plateau" region (Fig. 5.4), that is absent when the resonance is not excited.

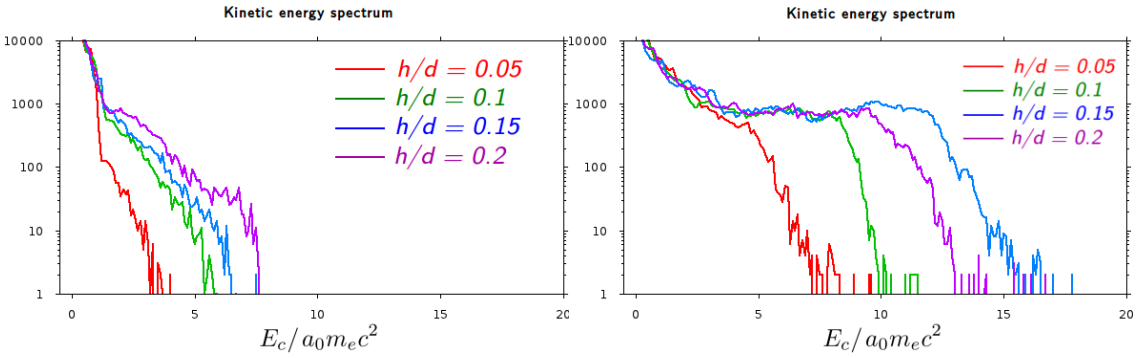

(a) *Out of resonance:* $\omega/\omega_0 = 1.1$ (b) *At resonance:* $\omega/\omega_0 = 0.98$

Figure 5.4: Logarithmic electrons' energy distribution for different values of h/d ratio. The average energy increase is clearly visible and doesn't depend on the grating depth

This confirms our hypothesis that the major effect in particle acceleration increase by the introduction of a structured surface target is due to the possibility to excite collective surface electrons modes, and cannot be simply explained as a consequence of hot spot creation in the field pattern in front of the target, because of bending of the field lines due to the modulation of the surface. Eventually, we have shown that for normal incident light the acceleration process can be ascribed to a $\mathbf{J} \times \mathbf{B}$ heating mechanism, while for oblique incidence it can be attributed to the "Brunel effect". This means that the introduction of a structured target results in a great enhancement of electrons acceleration due to SPR excitation without any substantial changes to the absorption mechanism.

5.2 Future directions

The extension of the analytical model to predict the resonant frequency shift derived in section 3.4 will be object of further study, for considering a two-modes only interaction is a limitation for the result precision.
Another limitation of this whole work is in the linear treatment of the optical response provided by the ionized material in front of the structured target. Indeed, when the intensity of the laser pulse goes much beyond the relativistic limit of $I \sim 10^{18} W/cm^2$ (nowadays pulses of the order of $10^{20 \div 21} W/cm^2$ are available) the dimensionless parameter a_0 becomes much greater than unity, therefore a fully non-linear treatment of the surface modes excitation is required.
The derivation of a model, even a rough one, to account for this non-linear optical response is crucial in order to continue to be able to predict with high accuracy the position of the plasmon resonance frequencies in the reflectivity spectrum, which are very sensitive to changes of the dielectric constant.
This investigation will be the main direction the authors will pursue in the near future.

Appendix A

FTDT method

The most general numerical methods for electromagnetism are those that simulate the full time-dependent Maxwell equations, propagating the fields in both space and time. Such time-domain methods can easily support strongly nonlinear or active (time-varying) media. Frequency-domain methods have more difficulty with those cases because frequency is not conserved. Time-domain methods can also be used solve the frequency-domain problems above, with some advantages and disadvantages as described below.

A.1 The finite-difference time-domain method

By far the most common technique for time-domain simulations is the finite-difference time-domain method, or FDTD. As the name implies, FDTD divides space and time into a grid (usually uniform) of discrete points and approximates the derivatives ($\nabla\times$ and $\partial/\partial t$) of the Maxwell equations by finite differences. The propagation in time, in particular, uses a "leap-frog" scheme where the $\mathbf{E}$ fields at time t are computed from the $\mathbf{E}$ fields at time $t-\Delta t$ along with the $\mathbf{H}$ fields at time $t-\Delta t/2$, and vice versa for $\mathbf{H}$ at $t+\Delta t/2$. In this way, the $\mathbf{E}$ and $\mathbf{H}$ field patterns are marched through time, offset by half of a time step Δt. Such a scheme provides a second order precision in the time domain. In order to obtain the same in the spatial domain we can use the same trick as in the temporal domain: in FDTD methods different field components are stored at different grid locations. This discretization grid is known as "Yee lattice".
The form of the Yee lattice in 3D is shown in the illustration A.1 for a single cubic grid voxel ($\Delta x\times\Delta x\times\Delta x$). The basic idea is that the three components of $\mathbf{E}$ are stored for the edges of the cube in the corresponding directions, while the components of $\mathbf{H}$ are stored for the faces of the cube:

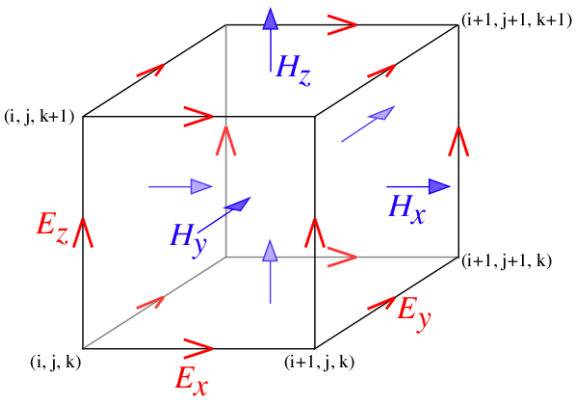

Figure A.1: Illustration of Yee lattice in 3d for a single grid voxel

In two dimensions, the idea is similar except that we set $\hat{\mathbf{e}}_z = 0$. The 2D Yee lattices for the TE polarizations (**E** in the xy plane and **H** in the z direction) is shown in the figure A.2

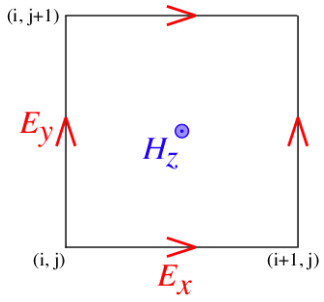

Figure A.2: Yee lattice in 2d for the TE polarization

For the TM polarizations, we just have to switch the electric with the magnetic field components.
The FDTD method is commonly employed to compute transmission and reflection spectra. Unlike solvers for a frequency-domain response, however, time-domain methods can compute the response of a linear system at many frequencies with a single computation. The trick is to take the Fourier transform of the response to a short pulse. For example, suppose you want to know the transmitted flux P through a plane as a function of frequency.

$$P(\omega) = \frac{1}{2}\text{Re}\ \hat{\mathbf{n}} \cdot \int \mathbf{E}_\omega(\mathbf{x})^* \times \mathbf{H}_\omega(\mathbf{x})\, d^2\mathbf{x} \tag{A.1}$$

You use an FDTD code to send a short pulse (which has a broad bandwidth) into the structure, and observe the resulting fields $\mathbf{E}(\mathbf{x}, t)$ and $\mathbf{H}(\mathbf{x}, t)$ at the output plane. These are Fourier-transformed to yield $\mathbf{E}_\omega(\mathbf{x})$ and $\mathbf{H}_\omega(\mathbf{x})$, from which the flux is obtained at each ω.
The power $P(\omega)$ by itself is not very useful, since one needs to normalize, dividing by the incident power at each frequency, to get the transmission spectrum. Typically, this is done by running the simulation twice: once with only the incident wave and no scattering structure, and once with the scattering structure, where the first calculation is used for normalization.
It gets more tricky if one wants to compute the reflection spectrum as well as the transmission. You can't simply compute the flux in the backwards direction, because this would give you the sum of the reflected and the incident power. You also can't simply subtract the incident power from backwards flux to get the transmitted power, because in general there will be interference effects (between incident and reflected waves) that are not subtracted. Rather, you have to subtract the Fourier-transformed incident fields $\mathbf{E}_\omega^{(0)}(\mathbf{x})$ and $\mathbf{H}_\omega^{(0)}(\mathbf{x})$ to get the reflected/scattered power:

$$P_r(\omega) = \frac{1}{2}\text{Re}\ \hat{\mathbf{n}} \cdot \int \left[\mathbf{E}_\omega(\mathbf{x}) - \mathbf{E}_\omega^{(0)}(\mathbf{x})\right]^* \times \left[\mathbf{H}_\omega(\mathbf{x}) - \mathbf{H}_\omega^{(0)}(\mathbf{x})\right] d^2\mathbf{x} \tag{A.2}$$

Again, you can do this easily in practice by running the simulation twice, once without and once with the scatterer, and telling the code to subtract the Fourier transforms in the reflected plane before computing the flux. And again, after computing the reflected power you will normalize by the incident power to get the reflection spectrum.
This is the technique we used so far to compute the reflectivity spectra throughout the whole thesis work. The typical simulation set up is shown in figure A.3

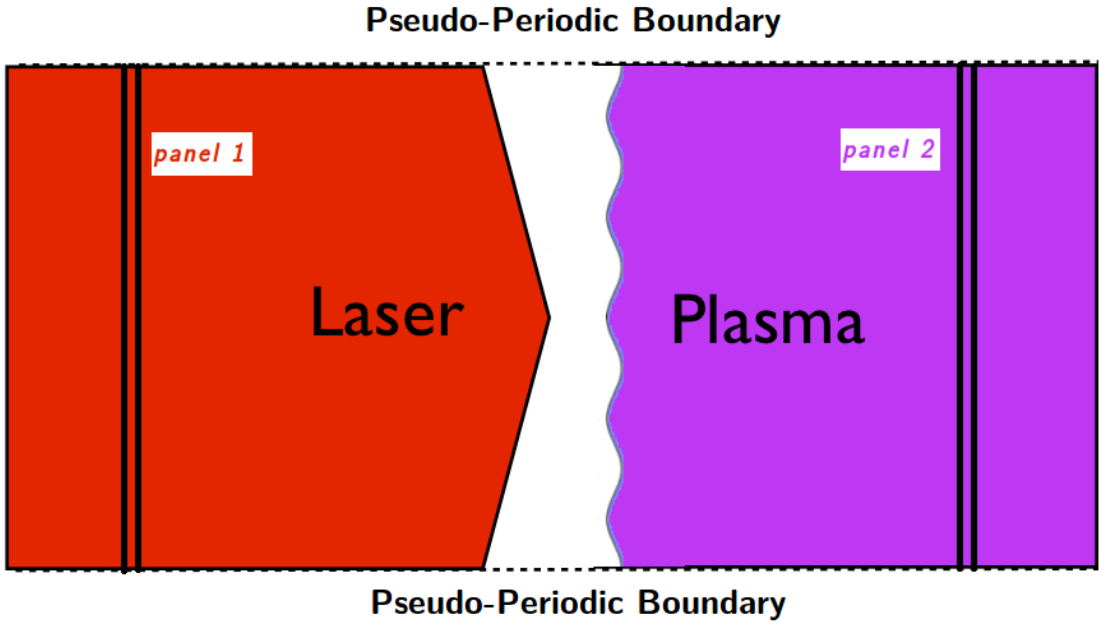

Figure A.3: Our simulation box

All the simulation regarding the electromagnetic part are made using a FDTD library called MEEP, see [Oskooi 2010].

A.2 A MEEP code example

What follows is the code I use to compute the interference pattern produced by a rough reflector, along with basic explanation.
The idea is to simulate a laser beam "entering" the simulation box from the bottom side, let it propagate towards a dielectric medium placed on the top side and impinge with an arbitrary incidence angle on the interface void/material. The simulation box is surrounded by a PML (Perfectly Matching Layer), a zone where the field amplitude is smoothed to zero in order to "absorb" the outgoing reflected wave without undesired backwards reflection. This is useful to analyse our problem in steady state.
To obtain this without much pain I use a libraries package developed at MIT to model electromagnetic systems. Its name is Meep (or MEEP) and is based on finite-difference time-domain (FDTD) technique. Furthermore, it's free. To install it on Ubuntu (or Debian) just type:

```
sudo apt-get install meep h5utils
```

It will install the whole package and other utilities to handle the output (hdf5 files).
To use it with C++ you only have to include the libraries and link the compiler to them.

```
#include <iostream>
#include <complex>
#include <meep.hpp>
using namespace std;
using namespace meep;
```

Then, I specify the physical properties of the problem, bearing in mind that in Meep units are specified in cgs system with $c = 1$. Thus, once specified a typical unit length a, all the other physical quantities are defined as follow: time in unit of $a/c = a$, frequency in $1/a$ as well as wave number. In my simulation I set $\lambda = 1\mu m$ and use it as reference for all other quantities (see comments on original code):

```
double wavelength = 1.0;
double fcen = 1.0/wavelength, fwidth = 0.5;
double k = fcen;
double w0 = 4.0/fcen;
double zr = pi*w0*w0/wavelength;
double angle = 90;
double theta = angle * pi/180;
double kx = k * cos(theta);
double ky = k * sin(theta);

vec K(kx,ky);
vec K_a(-ky,kx);

complex<double>i = sqrt( complex<double>(-1) ) ;
vec pos(0.0,19.0);
double sx = 35, sy = 18, dpml = 1.0;
double y_ant = 1.0;
double Amp = 0.25;
double q = 0.5;
```

It's important to know that in Meep the time harmonic dependence for a given f is expressed as $e^{-2\pi ift}$, so one doesn't have to define quantities such as k and ω with the factor 2π.
Now I specify the dielectric properties I want. Here I define two options: the first is to use a perfect electric conductor, the second a real overdense plasma (with no collisional absorption). In the first case I define a function ϵ that return a big negative number if a point $p = (p_x, p_y)$ is in the dielectric medium and 1 elsewhere.
In the second case I use a the predefined function add-polarizability() of the meep::structure object (see below) to create the dielectric function:

$$\epsilon(\omega) = 1 - \frac{\omega_p^2}{\omega^2}$$

The add-polarizability() function asks for the following arguments

```
meep::Structure::add_polarizability( double sigma(const vec &p),
                                     double w,
                                     double gamma )
```

in order to implement the dielectric function:

$$\epsilon(\omega) = \epsilon + \frac{w^2\sigma}{w^2 - \omega^2 - i\omega\gamma}$$

Thus, since I'm in the particular condition $n_c/n = \omega_p^2/\omega^2 = 25$, in order to implement my dielectric function I set $(\epsilon = 1, \gamma = 0, w = 0.01, \sigma(\mathbf{x}) = \omega^2 * 25/w^2)$

```
double interface(double x) {
return Amp*cos(2.0*pi*q*x);
}

double eps(const vec &p) {
// if (p.y() < sy+2*dpml && p.y() > sy + interface(p.x()))
// return -HUGE_VAL;
return 1.0;
}

double sigma(const vec &p) {
if (p.y() < sy+2*dpml && p.y() > sy + interface(p.x()))
return 250000*fcen*fcen;
return 1.0;
}
```

If I want to use a PEC I uncomment the content of the eps function and comment the sigma function, otherwise vice versa.
Next, I build a Gaussian beam using the paraxial approximation formula:

$$E(\xi,\eta) = \frac{w_0}{w(\xi)} \exp\left(-\frac{\eta^2}{w^2(\xi)}\right) \exp\left(-ik\xi - ik\frac{\eta^2}{R^2(\xi)} - i\zeta(\xi)\right)$$

where (ξ, η) are the beam natural axes. The functions w, R, ζ are the beam width, radius of curvature and Gouy phase shift.
To relate this formula to the coordinate system (x, y) I have to perform a translation of the origin to the waist point (specified by "pos") and a rotation of angle θ around the $\hat{z}$ axis passing through the waist point. This is given by:

$$\begin{pmatrix} \xi \\ \eta \end{pmatrix} = \begin{pmatrix} \cos\theta & \sin\theta \\ -\sin\theta & \cos\theta \end{pmatrix} \begin{pmatrix} x - x_w \\ y - y_w \end{pmatrix}$$

The implementation is straightforward:

```
double xi(const vec &p) {
return ((p.x()-pos.x())*K.x()+(p.y()-pos.y())*K.y())/k;
}

double eta(const vec &p) {
return ((p.x()-pos.x())*K_a.x()+(p.y()-pos.y())*K_a.y())/k;
}

double w(const vec &p) {
```

```
return w0*pow(1.0 + pow(xi(p)/zr,2.0), 0.5);
}

double zeta(const vec &p) {
return atan(xi(p)/zr);
}

double Radius(const vec &p) {
return xi(p)*(1.0 + pow(zr/xi(p),2.0));
}

complex<double> gauss(const vec &q) {
return w0/w(q)*exp(-pow(eta(q)/w(q), 2.0))*exp(2.0*i*pi*xi(q))*
*exp(2.0*i*pi*k*pow(eta(q),2.0)/Radius(q))*exp(i*zeta(q));
}

complex<double> plane(const vec &q) {
return exp(2.0*i*pi*(q & k));
}
```

In the main program I initialise Meep, define a computational grid-volume and the associated structure (describing the geometry and materials), initialise the fields, add sources, and then time-step.

```
int main(int argc, char **argv) {

initialize mpi(argc, argv);
double resolution = 20;
grid_volume v = vol2d(sx,sy+2*dpml, resolution);
```

The grid-volume class (declared in meep/vec.hpp) is a box of pixels; setting the resolution, i.e. the number of pixel per unit length, and the dimensions of the box, I specify the number of pixel in each direction. Furthermore, it stores different field components at different points (in order to keep track of the Yee lattice).
I pass this so-declared object as argument in meep::Structure constructor, as well as the dielectric function (and polarizability, when used) and the boundary condition.

```
s.add_polarizability(sigma,0.01,0.0);
```

I use the expression pml(dpml, Y) when I use plane waves, because in such case I have to set periodic boundary conditions on X sides, instead of absorbing conditions everywhere. To do so, after constructing the meep::fields object, I use the function use-bloch(vec &k), which makes the fields at one side be exp($i\mathbf{k}\cdot\mathbf{L}$) times the fields at the other side, assuming the sides separated by the lattice vector $\mathbf{L}$. So, setting $k = (0, 0)$, I simply obtain periodic boundaries in every direction. Since the geometry of the problems allows periodicity only along x, I set absorbing conditions on the y boundaries.

```
fields f(&s);
// f.use_bloch(vec(0,0));

f.output_hdf5(Dielectric, v.surroundings());
h5file *fileEx = f.open_h5file("ex",h5file::WRITE);
h5file *fileEy = f.open_h5file("ey",h5file::WRITE);
```

```
h5file *fileHz = f.open_h5file("hz",h5file::WRITE);
```

After creating the output files, I set sources of the EM fields. Firstly I create a meep::continuous-source-time object specifying as arguments the source frequency, the start up smoothing temporal function width (default is $f(t) = \tanh(df * t)$), and start/end times. Secondly, I create a meep::volume object which in 2d draws a line from the closest point to the origin to the farthest one. Eventually I add the sources to the f object through the meep::Fields class function .add-volume-source(), specifying as arguments which component to excite, with what physical properties, where, with which modulation and amplitude:

```
continuous_src_time src(fcen, fwidth, 0.0, infinity);
volume src_plane(vec(0.0,y_ant),vec(sx,y_ant));
f.add_volume_source(Ex, src, src_plane, gauss, 1.0);
```

Thus, with the lines above, I specified as source the x component of the electric field (p-polarization case), of frequency f, starting at $t = 0$ with a temporal ramp width df, emitted by an antenna placed at $y = 1$ with a spatial modulation given by the function gauss and amplitude $E_0 = 1$.

```
double T_end = 40;
while( f.time() < T_end ){
/* f.output_hdf5(Ex, v.surroundings(), fileEx, 1);
 * f.output_hdf5(Ey, v.surroundings(), fileEy, 1);
 * f.output_hdf5(Hz, v.surroundings(), fileHz, 1);
 */ f.step();
}
f.output_hdf5(Ex, v.surroundings(), fileEx);
f.output_hdf5(Ey, v.surroundings(), fileEy);
f.output_hdf5(Hz, v.surroundings(), fileHz);
```

Time-stepping and output of the computed EM fields. Note that the meep::Fields class function output-hdf5() provides the possibility to set the logical value of a boolean variable "append-data" (false by default). This allows one to record all the temporal steps of the computed fields in a unique file which will be a rank=3 tensor (index (x, y, t)) of data instead of a collection of (x, y) matrices for each time step.

Appendix B

Perturbative solution of the diffraction problem

S-polarisation case

In the case of s-polarisation the boundary condition is expressed as

$$F(x, \delta f(x), \delta) = -E_0\, e^{ik_x x - ik_y \delta f(x)} \tag{B.1}$$

In order to obtain the n^{th} components of field F we have to derivate n times expression B.1 with respect to δ. The left hand side reads

$$\frac{\partial^n}{\partial \delta^n} \left(F(x, \delta f(x), \delta)\right)_{\delta=0} = \sum_{\ell=0}^{n} \left(\begin{array}{c} n \\ \ell \end{array} \right) [f(x)]^{n-\ell} \frac{\partial^\ell}{\partial \delta^\ell} \left(\frac{\partial^{n-\ell} F}{\partial y^{n-\ell}}\bigg|_{y=0} \right)_{\delta=0} \tag{B.2}$$

By dividing both sides by $n!$ and remembering definition 2.36 we get

$$\begin{aligned} \frac{1}{n!}\frac{\partial^n}{\partial \delta^n} \left(F(x, \delta f(x), \delta)\right)_{\delta=0} &= \sum_{\ell=0}^{n} \frac{1}{n!} \frac{n!}{(n-\ell)!} [f(x)]^{n-\ell} \frac{1}{\ell!} \frac{\partial^\ell}{\partial \delta^\ell} \left(\frac{\partial^{n-\ell} F}{\partial y^{n-\ell}}\bigg|_{y=0} \right)_{\delta=0} \\ &= \sum_{\ell=0}^{n} \frac{f^{n-\ell}}{(n-\ell)!} \left. \frac{\partial^{n-\ell} F_\ell}{\partial y^{n-\ell}} \right|_{y=0} \end{aligned}$$

After derivating the right hand side of eq. B.1 and isolating the last term of the above series we eventually obtain:

$$F_n = ik_y \frac{(-ik_y f)^n}{n!} e^{ik_x x} - \sum_{\ell=0}^{n-1} \frac{f^{n-\ell}}{(n-\ell)!} \left. \frac{\partial^{n-\ell} F_\ell}{\partial y^{n-\ell}} \right|_{y=0} \tag{B.3}$$

Now, suppose that function $f(x)$ has a finite number of spectral components. Its Fourier expansion will be

$$f(x) = \sum_{r=-S}^{S} C_r e^{irqx} \tag{B.4}$$

since its period is d. Let $C_{\kappa,r}$ be the Fourier coefficients of the function:

$$\frac{f^\kappa}{\kappa!} = \sum_{r=-\kappa S}^{\kappa S} C_{\kappa,r}\, e^{irqx} \tag{B.5}$$

Use of equations 2.38 and B.5 in B.1 leads to:

$$\sum_r d_{n,r} e^{i\alpha_r x} = \sum_{r=-nS}^{nS} C_{n,r} \left[ik_x(-ik_y)^{n-1}(iqr) - (-ik_y)^{n+1} \right] e^{i\alpha_r x} + \\ - \sum_{\ell=0}^{n-1} \left\{ \left[\sum_{r=-(n-\ell)S}^{(n-\ell)S} C_{n-\ell,r}\, e^{iqrx} \right] \times \left[\sum_r d_{\ell,r}\, (i\beta_r)^{n-\ell} e^{i\alpha_r x} \right] \right\} \tag{B.6}$$

After resummation of the index in the sum signs we get:

$$\sum_r d_{n,r}\, e^{i\alpha_r x} = - \sum_{r=-nS}^{nS} C_{n,r}\, (-ik_y)^n e^{i\alpha_r x} + \\ - \sum_{\ell=0}^{n-1} \sum_{\kappa=-\infty}^{+\infty} \sum_{p=-(n-\ell)S}^{(n-\ell)S} C_{n-\ell,p} (i\beta_\kappa)^{n-\ell} d_{\ell,\kappa} e^{iqpx + i\alpha_\kappa x} \tag{B.7}$$

Now, setting $\alpha_{p+\kappa} = qp + \alpha_\kappa$ and changing p into $r - \kappa$ we get

$$\begin{aligned} \sum_r d_{n,r}\, e^{i\alpha_r x} &= - \sum_{r=-nS}^{nS} C_{n,r}\, (-ik_y)^n e^{i\alpha_r x} + \\ &\quad - \sum_{\ell=0}^{n-1} \sum_{\kappa=-\infty}^{+\infty} \sum_{r=\kappa-(n-\ell)S}^{\kappa+(n-\ell)S} C_{n-\ell,r-\kappa} (i\beta_\kappa)^{n-\ell} d_{\ell,\kappa} e^{i\alpha_r x} \qquad \text{or} \\ &= - \sum_{r=-nS}^{nS} C_{n,r}\, (-ik_y)^n e^{i\alpha_r x} + \\ &\quad - \sum_{r=-\infty}^{+\infty} \left[\sum_{\ell=0}^{n-1} \sum_{\kappa=r-(n-\ell)S}^{r+(n-\ell)S} C_{n-\ell,r-\kappa} (i\beta_\kappa)^{n-\ell} d_{\ell,\kappa} \right] e^{i\alpha_r x} \end{aligned} \tag{B.8}$$

Since $d_{\ell,\kappa} = 0$ if $|\kappa| > \ell S$, then the recursive formula takes the form:

$$d_{n,r} = -(-ik_y)^n C_{n,r} - \sum_{\ell=0}^{n-1} \sum_{\kappa=\max\{-\ell S, r-(n-\ell)S\}}^{\min\{\ell S, r+(n-\ell)S\}} C_{n-\ell,r-\kappa} (i\beta_\kappa)^{n-\ell} d_{\ell,\kappa} \tag{B.9}$$

B.1 P-polarisation case

Use of boundary condition 2.10 with argument similar to the one just described leads to the following relation:

$$i\beta_r d_{n,r} = (-ik_y)^{n-1}(k_y^2 - k_x rq) C_{n,r} + \\ + \sum_{\ell=0}^{n-1} \sum_{\kappa=\max\{-\ell S, r-(n-\ell)S\}}^{\min\{\ell S, r+(n-\ell)S\}} C_{n-\ell,r-\kappa} (i\beta_\kappa)^{n-\ell-1} \left[\beta_\kappa^2 - \alpha_\kappa (r-\kappa) q \right] d_{\ell,\kappa} \tag{B.10}$$

Appendix C

Fundamentals of high power laser matter interaction

C.1 Relativistic equations of motion

Although it is well known that the relativistic (covariant) motion of a charged particle in an electromagnetic field is described by

$$\frac{dp^\mu}{dt} = \frac{q}{c} F^{\mu\nu} u_\nu, \quad p^\mu = m\gamma u^\mu, \qquad F^{\mu\nu} = \partial^\mu A^\nu - \partial^\nu A^\mu \tag{C.1}$$

with A^μ the four-vector potential, it is always instructive to derive the three-dimensional version, which in our context is of more practical use, from classic mechanics principle. Thus, recalling that the energy of a relativistic particle is

$$E = m\gamma c^2 + V = \sqrt{m^2 c^4 + |\mathbf{p}|^2 c^2} + q\varphi$$

and that the canonical momentum is given by $\mathbf{P} = \mathbf{p} + q\mathbf{A}$, the relativistic Hamiltonian reads

$$H = mc^2 \sqrt{1 + \left(\frac{\mathbf{P}}{mc} - \mathbf{a}\right)^2} + q\varphi \tag{C.2}$$

with

$$\mathbf{a} = \frac{q\mathbf{A}}{mc^2}$$

being the dimensionless vector potential.
Then, from the canonical equations it follows that

$$\begin{cases} \dot{\mathbf{x}} = \dfrac{\partial H}{\partial \mathbf{p}} = \dfrac{\mathbf{P} - q\mathbf{A}}{m\sqrt{1 + \left(\frac{\mathbf{P}}{mc} - \mathbf{a}\right)^2}} \\ \dot{\mathbf{P}} = -\dfrac{\partial H}{\partial \mathbf{x}} = -\dfrac{1}{2m\gamma} \nabla (\mathbf{P} - q\mathbf{A})^2 - q\nabla\varphi \end{cases} \tag{C.3}$$

that can be rewritten as

$$\begin{cases} \dot{\mathbf{x}} = \dfrac{m\gamma \mathbf{u}}{m\gamma} = \mathbf{u} \\ \dot{\mathbf{P}} = -\dfrac{1}{m\gamma} [(\mathbf{P} - q\mathbf{A}) \times \nabla \times (\mathbf{P} - q\mathbf{A}) + (\mathbf{P} - q\mathbf{A}) \cdot \nabla (\mathbf{P} - q\mathbf{A})] - q\nabla\varphi \end{cases} \tag{C.4}$$

Thus, since $\mathbf{P} - q\mathbf{A} = m\gamma\mathbf{u}$ and $\nabla\mathbf{P} = 0$, the above equations finally simplify into

$$\begin{cases} \dot{\mathbf{x}} = \mathbf{u} \\ \dot{\mathbf{P}} = q\mathbf{u} \times \mathbf{B} + q(\mathbf{u} \cdot \nabla)\mathbf{A} - q\nabla\varphi \end{cases} \tag{C.5}$$

Thus, recalling that

$$\dot{\mathbf{P}} = \frac{d}{dt}(\mathbf{p} + q\mathbf{A}) = \frac{d}{dt}m\gamma\mathbf{u} + q\left[\frac{\partial \mathbf{A}}{\partial t} + (\mathbf{u} \cdot \nabla)\mathbf{A}\right] \tag{C.6}$$

and subsituting it in the second of equations C.5, we get:

$$\frac{d}{dt}m\gamma\mathbf{u} + q\left[\frac{\partial \mathbf{A}}{\partial t} + (\mathbf{u} \cdot \nabla)\mathbf{A}\right] = q\mathbf{u} \times \mathbf{B} + q(\mathbf{u} \cdot \nabla)\mathbf{A} - q\nabla\varphi \tag{C.7}$$

Since in Lorentz gauge

$$\mathbf{E} = -\frac{1}{c}\frac{\partial \mathbf{A}}{\partial t} - \nabla\varphi$$

The momentum equation eventually reads

$$\frac{d}{dt}(m\gamma\mathbf{u}) = q(\mathbf{E} + \mathbf{u} \times \mathbf{B}) \tag{C.8}$$

which is identical to the non-relativistic Lorentz's equation with the substitution $p = m\gamma u$ Moreover, from energy conservation we have that a time variation of the particle energy is due to thw work made by the fields on that particle, thus

$$\frac{d}{dt}(mc^2\gamma) = \mathbf{F}_L \cdot \mathbf{u} \tag{C.9}$$

which becomes:

$$\frac{d}{dt}mc^2\gamma = q\mathbf{u} \cdot \mathbf{E} \tag{C.10}$$

then, in summary, the energy momentum equation are:

$$\begin{cases} \dfrac{d\mathbf{p}}{dt} = q\left(\mathbf{E} + \dfrac{\mathbf{u}}{c} \times \mathbf{B}\right) \\ \dfrac{d}{dt}(m\gamma c) = \dfrac{q}{c}\mathbf{u} \cdot \mathbf{E} \end{cases} \tag{C.11}$$

which are respectively the spatial and temporal components of equation C.1.

C.2 Relativistic particle dynamics in vacuum

Let's consider the motion of an electron in a plane wave propagating along the x direction. The vector potential describing the plane waves can be chosen as

$$\mathbf{A} = \mathbf{e}_\perp A(x,t), \qquad \mathbf{k} \cdot \mathbf{A} = 0 \tag{C.12}$$

The last statement it's known as Coulomb gauge and corresponds to the setting of the gauge freedom by reducing the 4 degrees of freedom of four-vector potential A^μ to the two degrees of vector $\mathbf{A}_\perp$. This is required by the the fact that the e.m. field in vacuum has to be *transversal*, therefore the polarisation space is bi-dimensional.

Thus, the electric and magnetic fields are simply

$$\begin{cases} \mathbf{E} = -\partial_{ct}\mathbf{A} \\ \mathbf{B} = \nabla \times \mathbf{A} \end{cases} \tag{C.13}$$

Substituting in first of eq. C.11 we get:

$$\frac{d\mathbf{p}}{dt} = -e\left(-\partial_{ct}\mathbf{A} + \frac{\mathbf{u}}{c} \times \nabla \times \mathbf{A}\right) \tag{C.14}$$

Since

$$\mathbf{u} \times \nabla \times \mathbf{A} = \mathbf{u} \cdot (\nabla : \mathbf{A}) - (\mathbf{u} \cdot \nabla)\mathbf{A} \tag{C.15}$$

The above equation reads

$$\frac{d\mathbf{p}}{dt} = \frac{e}{c}\left(\frac{d\mathbf{A}}{dt} - \mathbf{u} \cdot (\nabla : \mathbf{A})\right) \tag{C.16}$$

where the dyadic tensor notation $(\nabla : \mathbf{A})_{ij} = \partial_i A_j$ is used.
If $\hat{x}$ is the direction of light propagation, then we can observe that:

$$\mathbf{u} \cdot (\nabla : \mathbf{A}) = \begin{pmatrix} \mathbf{u} \cdot \partial_x \mathbf{A} \\ 0 \\ 0 \end{pmatrix} \qquad (\mathbf{u} \cdot \nabla)\mathbf{A} = \begin{pmatrix} 0 \\ \mathbf{u} \cdot \nabla A_y \\ \mathbf{u} \cdot \nabla A_z \end{pmatrix} = (\mathbf{u} \cdot \nabla)\mathbf{A}_\perp \tag{C.17}$$

The equation C.11 can be split in a longitudinal and a transversal part:

$$\begin{cases} \dfrac{dp_x}{dt} = -\dfrac{e}{c}\mathbf{u} \cdot \partial_x \mathbf{A} \\ \dfrac{d}{dt}\left(\mathbf{p}_\perp - \dfrac{e}{c}\mathbf{A}\right) = 0 \end{cases} \tag{C.18}$$

The second equation just express the fact that $\mathbf{P}_\perp = \nabla_\perp H = 0$, i.e. the conservation of canonical momentum, while if the we combine the first equation with the second of eq. C.11, we get

$$\begin{cases} \dfrac{dp_x}{dt} = -\dfrac{e}{c}\mathbf{u} \cdot \partial_x \mathbf{A} \\ \dfrac{d}{dt}(m\gamma c) = -\dfrac{e}{c^2}\mathbf{u} \cdot \partial_t \mathbf{A} \end{cases} \implies \frac{d}{dt}(p_x - m\gamma c) = \frac{e}{c}\mathbf{u} \cdot \left(\frac{\partial}{\partial x} - \frac{1}{c}\frac{\partial}{\partial t}\right)\mathbf{A} \tag{C.19}$$

If we suppose $\mathbf{A}$ to be a plane travelling wave, then

$$\mathbf{A} = \mathbf{e}_\perp A(x,t) = \mathbf{e}_\perp A(x - ct) \quad \implies \quad \left(\frac{\partial}{\partial x} - \frac{1}{c}\frac{\partial}{\partial t}\right)\mathbf{A}(x - ct) = 0 \tag{C.20}$$

Thus we have obtained another conserved quantity:

$$m\gamma(u_x - c) = \alpha \tag{C.21}$$

$$\mathbf{p}_\perp - \frac{e}{c}\mathbf{A} = \mathbf{p}_{\perp 0} \tag{C.22}$$

If we imagine that for $t = -\infty$ there was no field and the particle was at rest, than we have

$$\begin{cases} m\gamma(u_x - c) = -mc \\ \mathbf{p}_\perp - \dfrac{e}{c}\mathbf{A} = 0 \end{cases} \implies \begin{cases} p_x = \gamma - 1 \\ p_\perp = \mathbf{a} \end{cases} \qquad p = \frac{\mathbf{p}}{mc} \tag{C.23}$$

Now we can observe that from the constraint

$$\begin{aligned} |\mathbf{p}|^2 + m^2c^2 = (m\gamma c)^2 \quad &\implies \quad |p|^2 + 1 = \gamma^2 \\ p_x^2 + p_\perp^2 + 1 &= \gamma^2 \\ \gamma^2 &= (\gamma - 1)^2 + |\mathbf{a}|^2 + 1 \\ \gamma &= 1 + \frac{|\mathbf{a}|^2}{2} \end{aligned} \tag{C.24}$$

This has two consequences:

- ▷ Relation between momentum components:

$$p_x = \frac{|\mathbf{a}|^2}{2} = \frac{|p_\perp|^2}{2} \quad \implies \quad p_x = \frac{\mathbf{p}_\perp}{2mc}$$

- ▷ Energy expression:

$$E = m\gamma c^2 = mc^2\left(1 + \frac{|\mathbf{a}|^2}{2}\right)$$

One has to be careful with the last expression: it doesn't express the amount of energy a particle can gain when accelerated by a plane wave. Actually, the hypothesis that $A(t = -\infty) = 0$ means that the wave was "turned on" at some moment in the past. This is very reasonable in the case of a wave-packet of finite duration, whose front reaches at some time the electron initially at rest. But after the packet has passed by, the momentum is again $\mathbf{p} = 0$, so that no net acceleration has occurred! This is a consequence of the more general Lawson-Woodward theorem (see [Lawson 1979]), which states that is impossible to accelerate a particle with an electromagnetic wave in vacuum.
Thus the above energy expression has be interpreted as the maximum acceleration a particle can undergo *while* moving in the external field.
It may be objected that looking at equation C.21 one can achieve acceleration simply introducing a constant term in the vector potential expression that doesn't appear in the real fields. This is wrong, since from the definition of vector potential in Coulomb gauge:

$$\mathbf{A} = -c\int_0^t \mathbf{E}(x,\tau)d\tau \tag{C.25}$$

thus, any constant non-zero term in the vector potential corresponds to a zero frequency harmonic in $\mathbf{E}$ field spectrum, which violates the radiation condition.

C.2.1 Particle motion in a monochromatic plane wave of constant arbitrary amplitude

If the wave is monochromatic, the vector potential can be expressed as follows:

$$\mathbf{A} = \mathbf{e}_\perp A(\phi), \quad \text{where } \phi = kx - \omega t \tag{C.26}$$

with

$$\mathbf{A}(\phi) = A_0 \left[0, \delta\cos\phi,\ \sqrt{1-\delta^2}\sin\phi\right] \tag{C.27}$$

Here $\delta \in [0,1]$, for $\delta = 0$ corresponds to circular polarization, $\delta = 1$ to linear. With definition C.27, the motion can be solved analytically (see [Gibbon 2005]):

$$\begin{cases} p_x = \dfrac{a_0^2}{4}\left[1 + (2\delta^2 - 1)\cos 2\phi\right] \\ p_\perp = a_0(\delta\cos\phi, (1-\delta^2)^{1/2}\sin\phi) \end{cases} \implies \begin{cases} kx(\phi) = \dfrac{a_0^2}{4}\left[-\phi - \left(\delta^2 - \dfrac{1}{2}\right)\sin 2\phi\right] \\ kr_\perp(\phi) = -a_0(\delta\sin\phi, (1-\delta^2)^{1/2}\cos\phi) \end{cases} \tag{C.28}$$

For linear polarisation, the trajectory of the accelerated electron is depicted in figure C.2

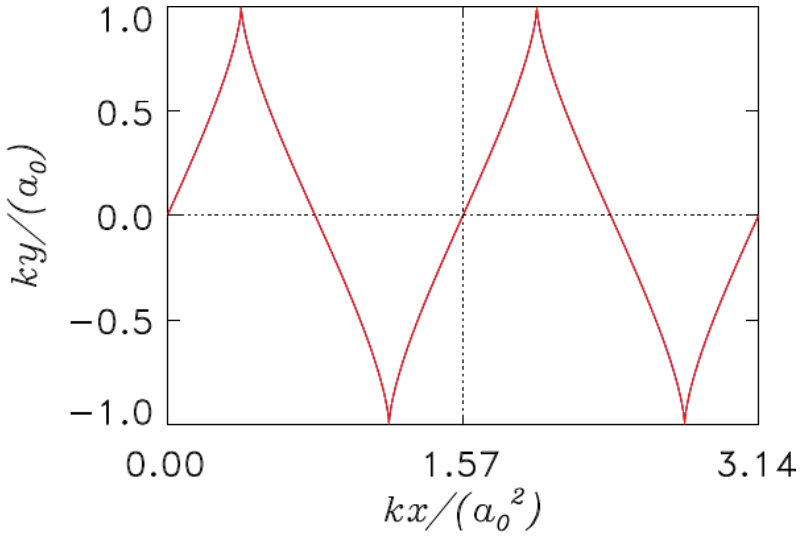

Figure C.1: Universal electron trajectory in plane wave

C.2.2 Average rest frame and ponderomotive potential

It is straightforward to observe that the underlying hypothesis in the previous section was that our wave was zero in a distant past and has been turned on adiabatically at some moment. This allows us to set $\alpha = -mc$, i.e. $\gamma_0 = \gamma(t=0) = 1$
However, in the steady state situation, we notice from equations C.28 that the transversal and longitudinal momentum components are both zero only for $\phi = \pm\pi/4$. Thus, if we want to study the "cycle-averaged" properties of the electron motion in an external plane wave, we should solve the momentum equations with steady-state initial conditions, and then carry out the average of the obtained quantities over a period $\phi \in [0, 2\pi]$.
Then, let's restart with equation C.23: since the only thing that changes here is substitution of $\alpha = -mc\gamma_0$ constant, we have:

$$\begin{cases} p_x = \dfrac{a^2}{2\gamma_0} \\ p_\perp = -\mathbf{a} \end{cases} \implies \begin{cases} \gamma\dfrac{dx}{cdt} = \dfrac{a^2}{2\gamma_0} \\ \gamma\dfrac{d\mathbf{r}_\perp}{cdt} = -\mathbf{a} \end{cases} \tag{C.29}$$

Observing that

$$\frac{d}{dt} = \frac{d\phi}{dt}\frac{d}{d\phi} = k(v_x - c)\frac{d}{d\phi}$$

and recalling that $m\gamma(v_x - c) = -mc\gamma_0$ we can rewrite the above equations as

$$\begin{cases} \dfrac{d(kx)}{d\phi} = -\dfrac{a^2}{2\gamma_0^2} \\ \dfrac{d(k\mathbf{r}_\perp)}{d\phi} = \dfrac{\mathbf{a}}{\gamma_0} \end{cases} \tag{C.30}$$

which are readily solved as before:

$$\begin{cases} kx(\phi) = -\dfrac{a_0^2}{4\gamma_0^2}\left(\phi + \dfrac{1}{2}\sin 2\phi\right) \\ k\mathbf{r}_\perp(\phi) = \dfrac{\mathbf{a}_0}{\gamma_0}\sin\phi \end{cases} \tag{C.31}$$

We notice immediately that while the transversal component of the motion is purely harmonic, the longitudinal components owns a secular term proportional to ϕ. Thus, if we consider only the average motion of the accelerated electron, or its guiding center motion, we find that:

$$\begin{aligned} \langle kx(\phi)\rangle \equiv k\bar{x} &= -\frac{a^2}{8\pi\gamma_0^2}\int_0^{2\pi}\left(\phi + \frac{1}{2}\sin 2\phi\right)d\phi \\ &= -\frac{a^2}{4\gamma_0^2}(k\bar{x} - \omega t) \\ \bar{x}\left(1 + \frac{a_0^2}{4\gamma_0^2}\right) &= \frac{a_0^2}{4\gamma_0^2}ct \\ \bar{x}(t) &= \frac{a_0^2}{4\gamma_0^2 + a_0^2}ct \end{aligned}$$

The guiding center moves with constant velocity $u_d = \frac{a_0^2}{4\gamma_0^2 + a_0^2}c$. Thus, it is possible to find a reference system where the guiding center is at rest, i.e. an "average rest" frame, in which the equations simply look like

$$\begin{cases} \gamma\dfrac{v_x}{c} = -\dfrac{a_0^2}{4\gamma_0}\cos 2\phi \\ \gamma\dfrac{v_\perp}{c} = a_0\cos\phi \end{cases} \quad\Longrightarrow\quad \begin{cases} kx(\phi) = -\dfrac{a_0^2}{8\gamma_0^2}\sin 2\phi \\ kr_\perp(\phi) = \dfrac{a_0}{\gamma_0}\sin\phi \end{cases} \tag{C.32}$$

Equations C.32 describe a figure-8 trajectory:

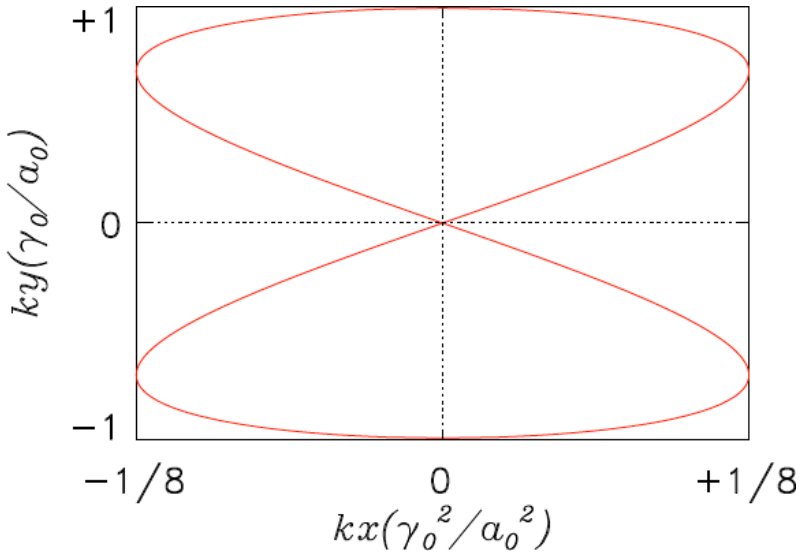

Figure C.2: Eight-like trajectory in the average rest frame

The constant γ_0 is conveniently determined for $\phi = \pi/4$, since $v_x(\pi/4) = 0$ and $v0 = v_\perp(\pi/4) = \frac{a_0 c}{\sqrt{2}\gamma_0}$. Hence,

$$\gamma_0 = \left(1 - \frac{v_0^2}{c^2}\right)^{-1/2} = \left(1 - \frac{v_\perp^2}{c^2}\right)^{-1/2} = \sqrt{1 + \frac{a_0^2}{2}} \tag{C.33}$$

The quiver motion around the guiding center in the average rest frame can be associated to a "quiver energy"

$$W = mc^2(\langle\gamma\rangle - 1) \tag{C.34}$$

which is the mean oscillation energy in the average rest frame. It is clear that averaging has to be done over the variable ϕ. By observing that:

$$\gamma\, d\phi = \gamma\, \frac{d\phi}{dt} dt = k\gamma(v_x - c)dt = -\gamma_0 d(\omega t) \tag{C.35}$$

the quiver energy becomes simply:

$$W = mc^2 \left(\sqrt{1 + \frac{a_0^2}{2}} - 1\right) \tag{C.36}$$

Now, imagine that $\mathbf{A}$ varies in space in such a way that $\partial_\phi A/|A| \ll 1$. Then, if for example we express the vector potential as $A = \hat{A}(\phi)\cos\phi$, W can be computed to first approximation just replacing all a_0 in the above formulas with $\hat{a}(\phi)$:

$$W = mc^2 \left(\sqrt{1 + \frac{\hat{a}^2(\phi)}{2}} - 1\right) \tag{C.37}$$

Thus now the quiver energy depends on the particle guiding center position (i.e. the slower motion component) which no longer moves with constant velocity. The question

arises as to where the energy change ΔW goes. Since a free electron can neither emit nor absorb photons of frequency (it can only scatter them) the only possibility is that the radiation field has done work on the free electron causing the motion of its oscillation center. Consequently, W is effectively a potential and its negative gradient is a force, the so-called ponderomotive force $\mathbf{f}_p$,

$$\mathbf{f}_p = -\nabla W = -mc^2 \nabla \hat{\gamma} \tag{C.38}$$

The above expression can be derived in a more rigorous way from variational principles, see for example [Bauer 1995]).

Bibliography

[Ashcroft 1976] Neil W. Ashcroft and N. David Mermin. Solid State Physics. Brooks Cole, 1 édition, January 1976. (Cited on page 27.)

[Atzeni 2004] S. Atzeni and J. Meyer-ter Vehn. The physics of inertial fusion. Oxford University Press, 2004. (Cited on page 3.)

[Bastiani-Ceccotti 2003] Serena Bastiani-Ceccotti, Patrick Monchicourt and Thierry Lehner. *Enhanced electronic emission by excitation of an interface resonance in metallic bilayer gratings irradiated by short laser pulses.* Phys. Rev. B, vol. 68, no. 24, page 245411, Dec 2003. (Cited on page 4.)

[Bauer 1995] D. Bauer, P. Mulser and W. H. Steeb. *Relativistic Ponderomotive Force, Uphill Acceleration, and Transition to Chaos.* Phys. Rev. Lett., vol. 75, no. 25, pages 4622–4625, Dec 1995. (Cited on page 68.)

[Bigongiari 2011] A. Bigongiari. *Laser-Overdense plasma coupling via Surface Plasma Waves and Steady Magnetic Field Generation.* Physics of Plasmas, in press, 2011. (Cited on page 5.)

[Borghesi 2006] M. Borghesi, J. Fuchs, S. V. Bulanov, A. J. MacKinnon, P. K. Patel and P. K. Roth. *Fast ion generation by high-intensity laser irradiation of solid targets and applications.* Fus. Sci. Techn., vol. 49, page 412, 2006. (Cited on page 3.)

[Born 1999] Max Born and Emil Wolf. Principles of Optics: Electromagnetic Theory of Propagation, Interference and Diffraction of Light. Cambridge University Press, 7th édition, October 1999. (Cited on page 23.)

[Brunel 1987] F. Brunel. *Not-so-resonant, resonant absorption.* Phys. Rev. Lett., vol. 59, no. 1, pages 52–55, Jul 1987. (Cited on page 3.)

[Bruno 1992] O. P. Bruno and F. Reitich. *Solution of a boundary value problem for Helmholtz equation via variation of the boundary into the complex domain.* Proc. R. Soc. Edinburgh A, vol. 122, pages 317–340, 1992. (Cited on page 14.)

[Bruno 1993a] Oscar P. Bruno and Fernando Reitich. *Numerical solution of diffraction problems: a method of variation of boundaries.* J. Opt. Soc. Am. A, vol. 10, no. 6, pages 1168–1175, Jun 1993. (Cited on page 14.)

[Bruno 1993b] Oscar P. Bruno and Fernando Reitich. *Numerical solution of diffraction problems: a method of variation of boundaries. II. Finitely conducting gratings, Padé approximants, and singularities.* J. Opt. Soc. Am. A, vol. 10, no. 11, pages 2307–2316, Nov 1993. (Cited on page 21.)

[Floquet 1883] G. Floquet. *Sur les équations différentielles linéaires à coefficients périodiques.* Annales scientifiques de l'É.N.S., vol. 12, pages 47–88, 1883. (Cited on page 9.)

[Gibbon 1992] Paul Gibbon and A. R. Bell. *Collisionless absorption in sharp-edged plasmas.* Phys. Rev. Lett., vol. 68, no. 10, pages 1535–1538, Mar 1992. (Cited on pages 3 and 46.)

[Gibbon 2005] Paul Gibbon. Short pulse laser interaction with matter. Imperial College Press, 2005. (Cited on page 65.)

[Hinkel-Lipsker 1991] D. E. Hinkel-Lipsker, B. D. Fried and G. J. Morales. *Conversion of electrostatic and electromagnetic waves in a plasma at the peak of a parabolic density profile.* Phys. Rev. Lett., vol. 66, no. 14, pages 1862–1865, Apr 1991. (Cited on page 23.)

[Irvine 2006] S. E. Irvine and A. Y. Elezzabi. *Surface-plasmon-based electron acceleration.* Phys. Rev. A, vol. 73, no. 1, page 013815, Jan 2006. (Cited on page 4.)

[J. Chandezon 1982] M. T. Dupuis J. Chandezon and G. Cornet. *Multicoated gratings: a differential formalism applicable in the entire optical region.* J. Opt. Soc. Am., vol. 72, no. 7, 1982. (Cited on page 17.)

[Kruer 1985] W. L. Kruer and Kent Estabrook. *J x B heating by very intense laser light.* Physics of Fluids, vol. 28, no. 1, pages 430–432, 1985. (Cited on page 3.)

[Kupersztych 2001] J. Kupersztych, P. Monchicourt and M. Raynaud. *Ponderomotive Acceleration of Photoelectrons in Surface-Plasmon-Assisted Multiphoton Photoelectric Emission.* Phys. Rev. Lett., vol. 86, no. 22, pages 5180–5183, May 2001. (Cited on page 4.)

[Lawson 1979] J D Lawson. *Lasers and Accelerators.* Nuclear Science, IEEE Transactions, vol. 26, no. 3, pages 4217 –4219, june 1979. (Cited on pages 2, 13 and 64.)

[Liu 2007] C. S. et al. Liu. *Electron acceleration by surface plasma waves in double metal surface structure.* AIP, vol. 102, no. 11, page 113301, 2007. (Cited on page 4.)

[Macchi] A. Macchi, T. Ceccotti and al. Ultrahigh contrast laser interaction with structured targets. SLIC UHI laser facility, CEA (France). Code: SLIC001693. (Cited on page 5.)

[Maier 2007] Stefan A. Maier. Plasmonics: Fundamentals and Applications. Springer, 1 édition, May 2007. (Cited on pages 1 and 24.)

[Maystre 1984] D. Maystre. *I Rigorous Vector Theories of Diffraction Gratings.* volume 21 of *Progress in Optics*, pages 1 – 67. Elsevier, 1984. (Cited on page 22.)

[McDonald] K. McDonald. *The grating accelerator.* (Cited on pages 11 and 13.)

[Mourou 1985] G. Mourou and D. Strickland. *Compression of amplified chirped optical pulses.* Opt. Commun., vol. 56, pages 219–221, 1985. (Cited on page 35.)

[Oskooi 2010] A. F. Oskooi. *Meep: A flexible free-software package for electromagnetic simulations by the FDTD method.* Computer Physics Communications, vol. 181, no. 3, pages 687 – 702, 2010. (Cited on page 53.)

[Palmer 1980] Robert B Palmer. *A Laser Driven Grating Linac.* Part. Accel., vol. 11, no. Print-80-0475, pages 81–90. 28 p, May 1980. (Cited on page 2.)

[Plettner 2005] T. Plettner. *Proof-of-principle experiment for laser-driven acceleration of relativistic electrons in a semi-infinite vacuum.* Phys. Rev. ST Accel. Beams, vol. 8, 2005. (Cited on page 3.)

[R. Dusseaux 1995] C. Faure R. Dusseaux and J. Chandezon. *New perturbation theory of diffraction gratings and its application to the study of ghosts.* J. Opt. Soc. Am. A, vol. 12, no. 6, 1995. (Cited on page 18.)

[Rayleigh 1907] Lord Rayleigh. *On the dynamic theory of gratings.* Proc. R. Soc. London Ser. A, vol. 79, pages 399–416, 1907. (Cited on page 10.)

[Raynaud 2007] M. Raynaud, J. C. Adam J. Kupersztych C. Riconda and A. Héron. *Strongly enhanced laser absorption and electron acceleration via resonant excitation of surface plasma waves.* Physics of Plasmas, vol. 14, page 092702, 2007. (Cited on page 4.)

[Smith 1953] S. J. Smith and E. M. Purcell. *Visible Light from Localized Surface Charges Moving across a Grating.* Phys. Rev., vol. 92, no. 4, page 1069, Nov 1953. (Cited on page 2.)

[Stockman 2007] M. I. Stockman, M. F. Kling, U. Kleineberg and F. Krausz. *Attosecond nanoplasmonic-field microscope.* Nature Photonics, vol. 1, no. 9, pages 539–544, 2007. (Cited on page 4.)

[Takeda 1968] Y. Takeda and I. Matsui. *Laser Linac with Grating.* Nucl. Instrum. Methods, vol. 62, page 306, 1968. (Cited on pages 2 and 13.)

[Veselago 1968] Viktor G. Veselago. *The electrodynamics of substances with simultaneously negative values of and.* Soviet Physics Uspekhi, vol. 10, no. 4, pages 509–514, April 1968. (Cited on page 24.)

[W. L. Barnes 1996] S. C. Kitson W. L. Barnes T. W. Preist and J. R. Sambles. *Physical origin of photonic energy gaps in the propagation of surface plasmons on gratings.* Phys. Rev. B, vol. 54, no. 9, 1996. (Cited on page 33.)

High Power Laser-Grating Interaction

Abstract:

In this work we study the application of surface plasmon resonances (SPR) in the field of high power laser-matter interaction in order to enhance the absorption process through light confinement near the target surface. First, the (SPR) properties are studied in the case in which the necessary momentum matching condition between the incident light wave-vector and the plasmon momentum is provided by a diffraction grating. We show that choosing the right wavelength, SPR can be excited even at normal incidence, and we derive a formula which allows us to predict the resonant frequency red-shift caused by increasing of the grating depth. Then, we show that the dynamics of the electrons produced by the material ionization, is greatly sensitive to SPR excitation. In particular, the average kinetic energy acquired by the electrons in the resonant fields is much greater than in the not resonant case. Thus, in laser interaction with a grating target, the great absorption enhancement found in previous works has to be ascribed to the excitation of SPR, for which the structured target surface behaves like an optical cavity.

Sommario:

In questo lavoro abbiamo studiato l'applicazione delle risonanze plasmoniche superficiali (RPS) al campo dell'interazione di laser di alta potenza con la materia, allo scopo di aumentare l'assorbimento di energia tramite iniezione di elettroni veloci confinando i campi elettromagnetici incidenti nei pressi della superficie del bersaglio. In un primo momento abbiamo illustrato le proprietà delle RPS quando la loro generazione (ovvero l'accoppiamento fotone-plasmone) è mediata dalla presenza di una modulazione periodica della superfice del bersaglio. Abbiamo mostrato che scegliendo opportunamente la lunghezza d'onda della radiazione incidente, è possibile eccitare i plasmoni superficiali anche ad incidenza normale, e in questa configurazione abbiamo derivato una formula che permette di predire lo spostamento verso il rosso delle lunghezze d'onda risonanti all'aumentare della profondità della modulazione. Dopodiché abbiamo mostrato come la dinamica degli elettroni prodotti per ionizzazione è fortemente sensibile alla presenza o meno di risonanze plasmoniche. In particolare, abbiamo osservato che l'energia cinetica che gli elettroni acquistano in media nel campo risonante è molto più alta che nel caso non risonante. Perciò, il grande incremento di assorbimento trovato nei precedenti lavori sull'interazione laser con bersagli dalla superficie modulata è da attribuirsi all'eccitazione delle risonanza plasmoniche superficiali, in corrispondenza delle quali il bersaglio si comporta come una cavità ottica.

Keywords:

laser-grating interaction, absorption enhancement, SPR excitation via grating, red-shift of resonant frequencies